HHS Public Access

Author manuscript

Cell Rep. Author manuscript; available in PMC 2024 July 22.

Published in final edited form as:

Cell Rep. 2024 June 25; 43(6): 114297. doi:10.1016/j.celrep.2024.114297.

FAK regulates tension transmission to the nucleus and endothelial transcriptome independent of kinase activity

Md Zahid Akhter[1], **Pascal Yazbeck**[1], **Mohammad Tauseef**[1], **Mumtaz Anwar**[1], **Faruk Hossen**[2], **Sayanti Datta**[1], **Vigneshwaran Vellingiri**[1], **Jagdish Chandra Joshi**[1], **Peter T. Toth**[1,3], **Nityanand Srivastava**[1], **Stephen Lenzini**[1], **Guangjin Zhou**[4], **James Lee**[2], **Mukesh K. Jain**[5], **Jae-Won Shin**[1,2], **Dolly Mehta**[1,6,*]

[1]Department of Pharmacology & Regenerative Medicine and Center for Lung and Vascular Biology, Chicago, IL, USA

[2]Department of Biomedical Engineering, Chicago, IL, USA

[3]Research Resources Center, University of Illinois, Chicago, IL, USA

[4]Department of Population and Quantitative Health Sciences, School of Medicine, Case Western Reserve University, Cleveland, OH, USA

[5]Division of Biology and Medicine, Warren Alpert Medical School, Brown University, Providence, RI, USA

[6]Lead contact

SUMMARY

The mechanical environment generated through the adhesive interaction of endothelial cells (ECs) with the matrix controls nuclear tension, preventing aberrant gene synthesis and the transition from restrictive to leaky endothelium, a hallmark of acute lung injury (ALI). However, the mechanisms controlling tension transmission to the nucleus and EC-restrictive fate remain elusive. Here, we demonstrate that, in a kinase-independent manner, focal adhesion kinase (FAK) safeguards tension transmission to the nucleus to maintain EC-restrictive fate. In FAK-depleted ECs, robust activation of the RhoA-Rho-kinase pathway increased EC tension and phosphorylation of the nuclear envelope protein, emerin, activating DNMT3a. Activated DNMT3a methylates the *KLF2* promoter, impairing the synthesis of *KLF2* and its target *S1PR1* to induce the leaky EC transcriptome. Repleting FAK (wild type or kinase dead) or inhibiting RhoA-emerin-DNMT3a activities in damaged lung ECs restored *KLF2* transcription of the restrictive EC

*Correspondence: dmehta@uic.edu.

AUTHOR CONTRIBUTIONS

M.Z.A. and D.M. designed the experiments. M.Z.A., P.Y., M.T., M.A., F.H., S.D., V.V., J.C.J., N.S., S.L., G.Z., and J.-W.S. performed the experiments and analyzed data. P.T.T. analyzed the image data. J.L. and M.K.J. provided reagents. M.Z.A. and D.M. wrote the manuscript. M.A., S.D., V.V., J.C.J., G.Z., J.L, M.K.J., and J.-W.S. commented on the manuscript.

DECLARATION OF INTERESTS

The authors declare no competing interests.

SUPPLEMENTAL INFORMATION

Supplemental information can be found online at https://doi.org/10.1016/j.celrep.2024.114297.

transcriptome. Thus, FAK sensing and control of tension transmission to the nucleus govern restrictive endothelium to maintain lung homeostasis.

In brief

The adhesive interaction between endothelial cells (ECs) and the matrix generates restrictive endothelium but the mechanism remains unclear. Akhter et al. show that, in a kinase-independent manner, FAK suppression of the RhoA pathway safeguards tension transmission to the nucleus, limiting emerin-DNMT3a activities and enabling *KLF2* transcription of the restricted ECs for vascular homeostasis.

Graphical Abstract

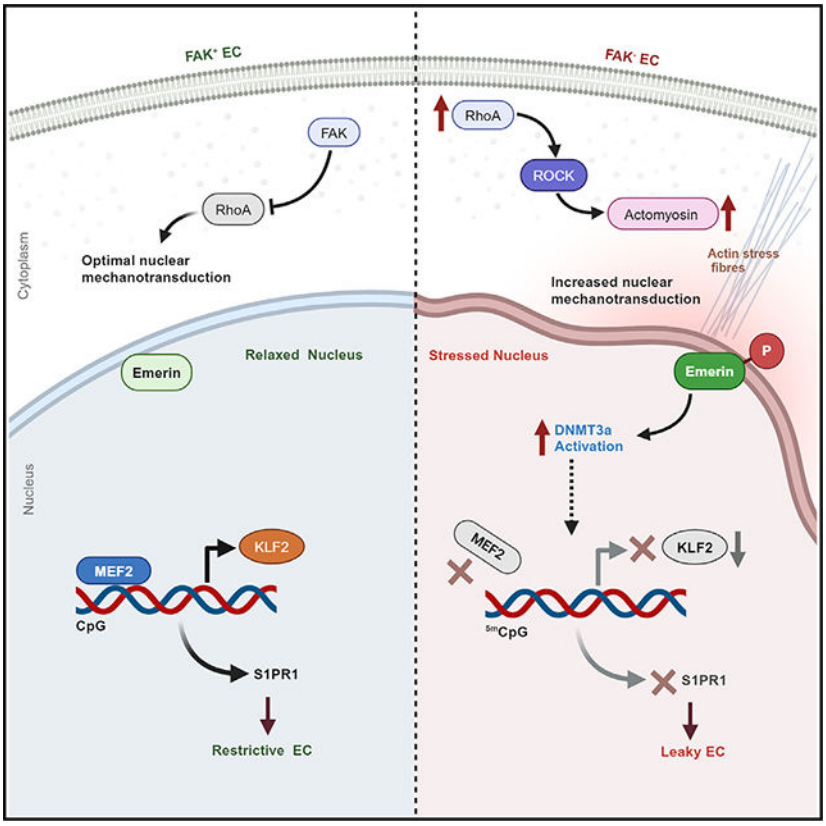

INTRODUCTION

Vascular endothelium maintains tissue-fluid homeostasis by restricting the passage of plasma proteins and blood cells to the underlying tissue.[1] Mechanical forces generated in endothelial cells (ECs) through their attachment to the extracellular matrix (ECM) function as key regulators of nuclear tension and EC-gene transcription.[1,2] However, the mechanisms that control tension transmission to the nucleus, thereby preventing conversion from restrictive to leaky EC phenotype, a hallmark of tissue injury, remain poorly understood. Identifying these tension-guarding mechanisms in ECs is critical to reversing the leaky EC

fate and lethal inflammatory diseases such as acute lung injury (ALI), acute respiratory distress syndrome (ARDS), and COVID-19.[3,4]

Focal adhesion kinase (FAK) was initially discovered in fibroblasts and chicken embryonic cells as the non-membrane-spanning tyrosine kinase linking cells to ECM proteins such as fibronectin at focal adhesions (FAs).[5] FAK was later shown to signal downstream of diverse receptors, including growth factors and G-protein-coupled receptors.[1,6–8] FAK activity is controlled through intramolecular interaction between four-point-one, ezrin, radixin, moesin (FERM) and the kinase domain.[9] FAK recruitment at FAs leads to FAK autophosphorylation at Y397, which allows its binding with Src-family kinases, leading to phosphorylation of residues Y576/Y577 and activation of FAK catalytic activity.[10] However, depending on the cellular context, FAK plays a multifaceted role in various cell types.[11] In cancer-associated fibroblasts and ECs, the elevation of FAK expression and kinase activity promotes cell adhesion, migration, invasion, and resistance to apoptosis,[12,13] leading to aggressive behavior and metastatic potential of cancer cells.[14] Pharmacologic or genetic inactivation of FAK activity (kinase dead [KD]-FAK) within fibroblasts dramatically reduces the spread of primary tumors.[15] Thus, FAK inhibitors are being touted as an anti-cancer therapy.

However, in ECs, FAK activation is linked with barrier formation by suppressing RhoA activity and VE-cadherin intercellular adhesions.[1,16–18] Thus, conditional FAK deletion in ECs induces vascular damage mimicking ALI.[19,20] Studies also suggest that FAK regulates EC functions in a kinase or kinase-independent manner, such as proliferation and migration through the FAK N-terminal FERM domain.[21] Using EC-specific KD-FAK knockin mice in ECs, Zhao et al. reported kinase-independent functions of FAK in regulating EC survival and their barrier function, which are critical for vascular development and functions.[22] Furthermore, recent studies demonstrated FAK to be a versatile scaffold that can localize in the nucleus and control gene transcription and cellular functions in a kinase-independent manner.[23,24] Thus, precisely how FAK functions to govern EC-restrictive fate remains to be seen.

The computer modeling and cellular studies suggest that FAK can directly sense the force perturbations applied to the FERM domain or FA, indicating that it serves as a mechanosensor.[25,26] Therefore, we tested the hypothesis that FAK is an intrinsic tension-transmission-guarding mechanism in ECs, through which nuclear tension and EC-restrictive fate are maintained. Using the *EC-FAK*$^{-/-}$ and wild-type (WT) mouse models combined with a multipronged approach, we identified FAK control of intracellular tension transmission in ECs as a critical determinant of nuclear mechanotransduction, which instructs the EC transcriptome in favor of a restrictive phenotype. We showed that this function of FAK occurs in a kinase-independent manner and involves suppression of the nuclear envelope protein, emerin, and DNMT3a activities to maintain *KLF2* transcription of restrictive EC fate and lung vascular homeostasis.

RESULTS

FAK softens ECs to maintain KLF2 expression and lung vascular homeostasis

Because the transition of ECs from a soft to a stiff state disrupts endothelial barrier function,[27] we assessed whether FAK, which maintains vascular barrier during development[22] and in adult endothelium,[19] functioned via softening ECs. We used atomic force microscopy (AFM) to quantify intracellular tension (i.e., Young's modulus [E]) in control versus FAK-depleted ECs.[28,29] We found that control ECs generate physiologically relevant intracellular EC tension of around ~800 Pa; however, tension increased significantly in FAK-depleted ECs (Figures 1A and S1A). As expected, FAK depletion also altered barrier permeability, which was determined by measuring transendothelial electrical resistance (TEER) across the monolayer in real time (Figure S1B).[30] Additionally, we depleted FAK using another FAK targeting small interfering RNA (siRNA) (siFAK-2) to rule out the non-specific effects of siRNA on EC tension. We found that siFAK-2 also increased EC stiffness and barrier permeability (Figures S1C–S1E).

In other studies, we quantified cytoskeletal tension induced by loss of FAK in ECs using the collagen gel contraction assay. FAK-depleted ECs generated much more contraction (~23%) than control ECs, which generated only ~1% contraction (Figures 1B, 1C, and S1F), corroborating findings that FAK depletion stiffens ECs.

RhoA via Rho kinase mediates myosin light-chain phosphorylation (MLC).[16,19,31] Because FAK suppresses the RhoA pathway,[32] we determined whether activation of RhoA increases EC tension in FAK-depleted ECs. First, we quantified tension in ECs overexpressing GFP-tagged WT-RhoA, constitutively active (CA) RhoA (Q63L), or dominant-negative (DN) RhoA (T19N) mutants. ECs expressing WT or CA-RhoA developed more tension than the DN-RhoA-ECs (Figure S1G). Consistent with these observations, inhibition of myosin-II activity[33] or Rho-kinase activity[34] in FAK-depleted ECs reversed tension to the level seen in control ECs (Figure 1D).

Evidence indicates that FAK can regulate EC functions independent of its kinase activity.[19,21,22] Therefore, we transduced the WT-FAK or KD-FAK (K454R)[26,32,35] mutants in FAK-depleted ECs and determined stiffness, RhoA activity, and MLC phosphorylation. WT- and KD-FAK rescued EC stiffness in FAK-depleted ECs to the level observed in control cells (Figures 1E and S1H). In a kinase-independent manner, FAK also suppressed RhoA activity (Figure S1I) and MLC phosphorylation (Figure S1J). In line with these findings, the expression of DN-RhoA in FAK-depleted ECs rescued EC stiffness and MLC phosphorylation (Figures 1E and S1J).

We, therefore, assessed the causal role of FAK in maintaining vascular homeostasis and whether this required the kinase activity of FAK. We injected tamoxifen in *FAK*$^{fl/fl}$ and *EC-FAK*$^{-/-}$ mice) to delete FAK specifically in ECs, as described[19,30,36] (Figure S2A), and found that FAK deletion in ECs increased edema in the lung but not in the heart, liver, or kidney (Figures S2B–S2F), indicating EC-FAK deletion primarily affected the pulmonary circulation but not the systemic circulation. Next, we inserted WT-FAK and KD-FAK cDNAs with the Cdh5 (VE-cadherin)-driven promoter to express FAK (WT- or

KD-FAK) only in ECs of *EC-FAK*$^{-/-}$ mice[37] (Figure 1F). We confirmed the delivery of these liposome nanoparticles in the lungs using immunoblotting and immunohistochemistry (Figures S2G–S2I). We found that WT- and KD-FAK rescued lung homeostasis, while this response was not seen in EC-FAK-null mice transducing vector alone (Figure 1G). Next, we flow-sorted ECs and non-ECs using anti-CD31 and anti-CD45 antibodies from the lungs of *EC-FAK*$^{-/-}$ mice and control mice receiving WT-FAK, KD-FAK, and vector cDNA constructs (Figure S3A). We assessed the expression of FAK, MLC phosphorylation as a readout of RhoA activity, and VE-cadherin phosphorylation as an indicator of intercellular junction integrity. We also found that WT- and KD-FAK were expressed in EC-FAK-null lungs to the level observed in control lungs (Figure S3B). As expected, FAK was not expressed in the lungs receiving vector alone (Figure S3B). We also showed that FAK was phosphorylated in EC-FAK-null lungs receiving WT-FAK cDNA but not in lungs receiving vector or KD-FAK mutant (Figure S3B). Consistently, loss of FAK increased MLC and VE-cadherin phosphorylation in ECs sorted from the EC-FAK-null lungs receiving vector alone but not the lungs receiving WT-FAK or FD-FAK mutants (Figure S3B). These data also show that liposomes were specifically delivered to ECs of the lungs since we did not find any alteration in FAK expression in non-EC compartments sorted from control lungs versus EC-FAK-null lungs receiving indicated cDNA constructs (Figure S3C). These data established the specificity of gene delivery to ECs of lungs using liposomes and that FAK directly regulates EC tension by suppressing the RhoA pathway in a kinase-independent manner to maintain restrictive EC and basal lung-fluid homeostasis.

Mechanical tension influences proper chromatin assembly and gene transcription to regulate cell fate.[38] We assessed whether increased intracellular tension seen in FAK-depleted ECs is conveyed to the nucleus via actomyosin filaments. We found that the actin stress fibers contact the nucleus in FAK-depleted cells but not in control ECs (Figures S3D and S3E). Therefore, we addressed the impact of FAK maintenance of EC tension in regulating chromatin accessibility to transcription factors and their roles in governing EC fate. We sorted ECs from *tdTom-EC* and *tdTom-EC-FAK*$^{-/-}$ mice (Figure S4A) and performed an assay of transposase accessible chromatin with sequencing (ATAC-seq) to identify the tension-sensitive transcription factors regulating FAK-driven cell responses (Figures 1H and S4A–S4C). Findings showed that the chromatin regions linked with the *KLF2*, *SOX17*, and *FOXP1* transcription factors were accessible in FAK^{+} ECs but not FAK^{-} ECs (Figures 1I, S5A, and S5B). We validated these findings in FAK^{+} or FAK^{-} sorted ECs (Figure S5C). Similarly, FAK-depleted human ECs showed reduced expression of *KLF2*, *SOX17*, and *FOXP1* (Figure S5D), indicating that FAK is required to facilitate the accessibility of their promoters and gene synthesis.

Next, we depleted KLF2, FOXP1, and SOX17 in ECs and determined barrier function (TEER) to identify the transcription factors that phenocopy the findings in FAK-depleted ECs.[16,19,32] We found that depletion of KLF2 markedly reduced TEER; i.e., it disrupted EC barrier function much like that seen in FAK-depleted ECs (Figures 1J and S5E). In contrast, depletion of SOX17 or FOXP1 had a modest effect on TEER (Figures S5F–S5H). Restoration of KLF2 expression in FAK-depleted ECs rescued EC barrier function (Figures 1K and S5I). As expected, rescuing SOX17 expression barely affected EC barrier dysfunction in FAK-depleted ECs (Figures S5J and S5K).

To assess whether matrix stiffness similarly alters *KLF2* expression, we plated ECs on soft (~3 kPa) versus stiff (~20 Kpa) polyethylene glycol (PEG) hydrogels[39] and found that ECs plated on stiff PEG showed reduced *KLF2* expression compared with ECs plated on soft PEG (Figure S5L).

As in ECs, rescuing *KLF2* expression in ECs of EC-FAK-null lungs resolved lung edema (Figure 1L). Immunoblot analysis of lungs receiving KLF2-cDNA confirmed KLF2 delivery (Figure S5M). Thus, genome-wide chromatin accessibility of lung vessels identified KLF2 as the tension-regulated transcription factor downstream of FAK.

FAK maintains *KLF2* synthesis by suppressing methylation of *KLF2* promoter by DNMT3a

The *KLF2* promoter contains CpG islands between −524 and −343 in the promoter region (Figure 2A), which are the targets of DNA methyltransferases (DNMTs).[40] We tested the possibility that FAK maintains *KLF2* expression by suppressing methylation of *KLF2* promoter. Bisulfite conversion of genomic DNA showed the methylation states of individual cytosines on DNA molecules.[41] In FAK-depleted ECs, 72% of the DNA underwent bisulfite conversion, indicating a 3-fold increase in DNA methylation (Figures 2B and 2C), further confirmed by methylation-specific PCR using methylation specific primers listed in Table 1 (Figures 2D and 2E).

MEF2 synthesizes *KLF2* by binding to the *KLF2* promoter within the region containing CpG islands and, thus, sensitivity to DNA methylation.[40] Chromatin immunoprecipitation (ChIP) analysis revealed a 70% reduction in MEF2 binding to the *KLF2* promoter in FAK-depleted ECs compared to controls (Figures 2F and S6A), supporting the above findings that the methylated *KLF2* promoter is inaccessible to its transcription factor, thus impairing KLF2 synthesis.

DNMT1, DNMT3a, and DNMT3b process DNA methylation.[42] DNMT1 is involved in hereditary DNA methylation, while DNMT3a and 3b regulate *de novo* DNA methylation.[42] We found similar expression of DNMT1, DNMT3a, and DNMT3b in $FAK^{fl/fl}$ or $EC\text{-}FAK^{-/-}$ lungs (Figure S6B). However, DNMT3a activity was increased by a factor of ~2.5 in EC-FAK-null lungs (Figure 2G) and ~3–3.5 in FAK-depleted ECs (Figure 2H). We also analyzed the nuclear distribution of 5-methylcytosine (5-mC), a measure of DNMT activity, at the single-molecule level using specific 5-mC probes in conjunction with 3D stochastic optical reconstruction microscopy (STORM) in control versus FAK-depleted ECs. We found a ~3-fold increase in 5-mC fluorophores in the nuclei of FAK-depleted ECs over control ECs (Figures 2I and 2J). Immunostaining of control and FAK-depleted ECs with anti-methylcytosine antibody showed a 3-fold increase in 5-mC levels in the nuclei of FAK-depleted cells (Figures S6C and S6D). Next, we knocked down DNMT3a or DNMT3b in FAK-depleted ECs and found that the depletion of DNMT3a but not DNMT3b (data not shown) rescued DNMT activity to near control levels (Figures 2K and S6E).

Because activated FAK translocates into the nucleus and interacts with DNMT3a to alter gene methylation and cell differentiation,[23] we inhibited FAK using PF-562271.[24] However, we failed to find an increase in FAK localization within the nucleus or alteration in barrier function (Figures S6F and S6G). In line with these studies, injection of PF-562271 in WT

mice reduced FAK phosphorylation at Y397 but did not affect edema or FAK expression (Figures S6H and S6I). However, we found that transduction of WT-FAK or the KD-FAK mutant and DN-RhoA mutant in FAK-depleted cells subverted DNMT activity to the level seen in control cells (Figures S7A–S7C). Thus, FAK suppression of RhoA-mediated EC stiffening was crucial in safeguarding DNMT3a methylation of the *KLF2* promoter.

Inhibition of DNMT3a activity reverses KLF2 expression and EC fate from leaky to a restrictive phenotype

ALI is associated with decreased FAK and KLF2 expression.[19,20] To assess whether lipopolysaccharide (LPS) increased DNMT activity in WT mice and inhibition of DNMT3a activity would convert ECs from a leaky to restrictive phenotype by preserving KLF2 expression, we inhibited DNMT3a activity in mice specifically using theaflavin-3,3′-digallate (TF-3) (1 mg/kg, intravenously [i.v.]) and after 1 h induced endotoxemia (LPS, 10 mg/kg, intraperitoneally [i.p.]) (Figure 3A). LPS elevated DNMT activity (Figure 3B) in mice receiving vehicle alone but failed to increase DNMT3a activity in mice receiving TF-3 (Figure 3B). As expected, LPS decreased *FAK* and *KLF2* expression in the lungs (Figures 3C, S7D, and S7E). However, LPS failed to reduce *KLF2* expression in mice treated with TF-3, and these mice rapidly resolved lung edema (Figures 3C and 3D). We also assessed whether TF-3 could promote the resolution of lung injury if given after the LPS challenge (Figure S7F). We found that TF-3 significantly reduced lung edema formation (Figure S7G). Similarly, the knockdown of DNMT3a in FAK-depleted ECs reversed *KLF2* expression to control levels (Figure 3E). TF-3 and Pan-DNA methyltransferase inhibitor, 5-aza-2′-deoxycytidine (AZA) (0.5 mg/kg, i.v.), rescued *KLF2* expression in FAK-depleted ECs or EC-FAK-null lungs (Figures S7H–S7J).

If DNMT3a is responsible for subverting ECs into their leaky phenotype by downregulating *KLF2*, deleting *DNMT3a* in ECs of FAK-null mice should rescue gene expression and barrier function. Thus, we generated inducible EC-specific double-knockout (DKO) mice in which tamoxifen deletes FAK and DNMT3a in *FAK*/*DNMT3a*$^{cre\text{-}scl\text{-}ERT}$ (Figures 3F and S7K). In contrast to FAK, DNMT3a deletion alone in ECs did not alter vascular permeability in lungs at homeostasis (Figure 3G). However, deleting DNMT3a in ECs of *EC-FAK*$^{-/-}$ restored the lung vascular barrier (Figure 3G). TF-3 and AZA also reduced vascular hyperpermeability in *EC-FAK*$^{-/-}$ mice (Figure S7L). TF-3 addition also rescued the endothelial barrier and EC stiffening in FAK-depleted ECs to the level observed in control ECs (Figures 3I–3K).

We also quantified DNMT activity in ECs plated on stiff versus soft matrices and found a 4-fold increase in DNMT activity in ECs plated on the stiff matrix than in ECs plated on the soft matrix (Figure S7M). These findings, along with data in Figures 1 and 2, demonstrate that EC stiffening is a generalized phenomenon during vascular injury that, in turn, upregulates DNMT3a activity to compromise KLF2 synthesis and, thereby, EC fate.

KLF2 maintains restrictive EC fate by synthesizing S1PR1

We next flow-sorted ECs from control and EC-FAK-null lungs to assess the EC transcriptome dictating EC-restrictive fate and whether it required KLF2 for gene synthesis.

RNA sequencing (RNA-seq) analysis in FAK^{-} ECs identified *S1PR1*, a G-protein-coupled receptor that we previously showed maintains EC barrier function,[30] as the crucial gene is reduced in these ECs (Figure 4A). We used multipronged approaches to test the hypothesis that KLF2 synthesis of *S1PR1* maintains the EC-restrictive phenotype downstream of FAK. First, we determined S1PR1 expression at mRNA and protein levels in FAK-null ECs and found these significantly lower than the control ECs (Figures 4B and 4C). Depletion of FAK using siRNA 1 (siFAK) or 2 (siFAK-2) similarly showed significantly reduced expression of S1PR1 (Figures S8A–S8C). However, FAK depletion did not affect other S1P receptors in ECs, such as S1PR2 and S1PR3 (Figure S8D). Expression of either S1P-synthesizing enzymes, SPHK1 or SPHK2, or KLF4, which also maintains EC integrity, was not altered (Figure S8D).

S1P enhances basal barrier function in ECs and repairs lungs subjected to vascular injury.[30,43,44] Thus, we determined whether S1P addition would promote endothelial integrity in FAK-null ECs despite a ~50% reduction in *S1PR1* expression. S1P failed to resolve vascular barrier leak in *EC-FAK*$^{-/-}$ mice (Figure 4D). We also determined the effect of S1P in strengthening endothelial monolayer integrity by quantifying TEER in control monolayers and FAK-depleted or KLF2-depleted ECs. As expected, S1P enhanced barrier function, i.e., TEER in control ECs, but this response was not observed in FAK or KLF2-depleted ECs (Figures 4E, 4F, and S8E).

Next, we restored *S1PR1* expression by transducing S1PR1 cDNA in FAK-depleted ECs and found that restoration of *S1PR1* rescued basal and S1P-mediated increases in TEER (Figures 4G–4I). Based on these findings, we transduced S1PR1 cDNA driven by the Cdh5 promoter in ECs of EC-FAK-null mice as above and found that transduction of S1PR1 in lungs reversed the EC-restrictive fate in FAK-null mice (Figures 4J and S8F).

Because *in silico* analysis of the *S1PR1* promoter showed three KLF2 binding sites within the 1-kb promoter region of the mouse *S1PR1* gene[45] (Figure 5A), we co-transfected ECs with the WT-S1PR1 luciferase promoter or mutated S1PR1 (lacking KLF2 binding sites), luciferase promoter, and KLF2 cDNA and determined promoter activity. KLF2 induced the *S1PR1* promoter activity in WT-S1PR1 promoter-transducing ECs (Figure 5B) but not in ECs transducing the mutated S1PR1 promoter (Figure 5B). Further, depletion of KLF2 reduced *S1PR1* mRNA and protein expression (Figures 5C and 5D), and S1P failed to enhance EC barrier function in KLF2-depleted ECs (Figures 5E and S8E). Restoration of *KLF2* expression in FAK-depleted ECs rescued *S1PR1* expression and S1P enhancement of barrier function (Figures 5F and 5G). Restoring FAK expression (WT or KD) or inhibiting RhoA activity by the DN-RhoA mutant in FAK-depleted cells rescued KLF2 and S1PR1 levels similarly to control cells (Figures S8G–S8J). Moreover, restoration of KLF2 in FAK-depleted ECs rescued permeability and intracellular tension like the control cells (Figures 5H and 5I). Also, impairment of DNMT3a activity in FAK-depleted ECs reversed *S1PR1* expression (Figures 5J–5L). These data show that KLF2 functioned downstream of FAK by synthesizing *S1PR1*. The primers used for quantitative real time PCR in this study have been listed in Table 2.

Emerin activates DNMT3a to induce a leaky EC phenotype

The linker of nucleoskeleton and cytoskeleton (LINC) senses tension in the nuclear envelope.[46] Because emerin activation is linked with increased nuclear stiffening,[47] we tested the hypothesis that FAK maintains restrictive ECs by suppressing emerin activity. Immunostaining of control and FAK-depleted ECs using an anti-emerin antibody revealed diffuse emerin localization in control ECs (Figures 6A and 6B). However, in FAK-depleted ECs, emerin condensed into a nuclear cap (Figures 6A and 6B). Likewise, emerin formed a nuclear cap in ECs cultured on a stiff matrix rather than a soft one (Figures S9A and S9B).

Emerin undergoes tyrosine phosphorylation via tyrosine kinases such as cSrc upon sensing tension.[46,47] cSrc activation compensates for the loss of FAK function.[48] Thus, we next assessed whether loss of FAK in ECs activates emerin by inducing post-translational modification via cSrc. FAK depletion increased cSrc phosphorylation at Y419, a measure of cSrc activity[49] (Figure 6C). Rho-kinase inhibition reversed cSrc activity as in control cells (Figure 6C). Compared to control ECs, FAK depletion enhanced emerin tyrosine phosphorylation by ~2.5-fold (Figure 6D). Inhibition of Rho kinase and cSrc restored emerin phosphorylation in FAK-depleted cells in a manner equivalent to control cells (Figure 6D). The above findings identify emerin as a novel target of FAK and suggest that FAK control of intracellular tension transmission to the nuclear envelope is required to suppress emerin activation.

Emerin tyrosine phosphorylation at Tyr74 and Tyr95 regulates nuclear stiffening.[47] Therefore, we examined the effects of disrupting emerin phosphorylation at these residues (Y74F/Y95F) on DNMT activity, gene expression, and EC fate in FAK-depleted cells. First, we overexpressed mutated (Y74F/Y95F) or WT emerin in FAK-depleted ECs and assessed emerin organization. We found that mutated but not WT emerin reversed emerin expression in FAK-depleted ECs from the nuclear cap to diffuse one in the nucleus (Figures 6E and 6F). Emerin phosphorylation at Tyr 74/95 increased DNMT3a activity in FAK-depleted ECs since the phospho-defective emerin mutant rescued DNMT activity in FAK-depleted cells as in control cells (Figures 7A and S9C). This response was not seen in FAK-depleted ECs expressing WT emerin (Figures 7A and S9C). Transduction of phospho-defective emerin (Y74F/Y95F) restored KLF2 or S1PR1 expression and monolayer integrity as indicated by increased VE-cadherin expression and reduced intercellular gaps in FAK-depleted ECs (Figures 7B–7E). However, WT emerin failed to reverse these responses in FAK-depleted ECs (Figures 7B–7E). In line with these findings, the emerin mutant restored monolayer resistance and EC stiffening in FAK-depleted ECs (Figures 7F and 7G). In other studies, we probed nuclear contractility by micromanipulating nuclei in an AFM study. Data indicated that FAK depletion increases nuclear contractility, reduced in cells transducing phospho-defective but not WT emerin (Figure S9D). The results suggest that, in the absence of FAK, phosphorylated emerin is critical in mediating DNMT3a activity that suppresses *KLF2* synthesis of *S1PR1,* leading to the leaky EC fate.

DISCUSSION

The mechanisms controlling the re-establishment of the restrictive EC fate are the key to reversing diseases caused by leaky vasculature syndrome, including ALI.[1] Previous studies

demonstrated FAK as a mechanical tension sensor.[50] We showed that loss of FAK in ECs increases intracellular tension impinging on the nucleus, leading to emerin reorganization and tyrosine phosphorylation at Y74/Y95 in a RhoA-cSrc pathway-dependent manner. Phosphorylated emerin upregulated DNMT3a activity, leading to methylation of the KLF2 promoter, suppression of S1PR1 synthesis, and conversion of restrictive ECs to their leaky phenotype. However, delivery of either WT-FAK or the KD-FAK mutant in FAK-depleted ECs or ECs of EC-FAK-null mice subverted increased intracellular tension and DNMT3a suppression of *KLF2* synthesis and its transcriptional activity to normal levels, reversing the EC-restrictive phenotype. Thus, we have demonstrated the crucial role of FAK as a tension sensor and guardian of the EC transcriptome and phenotype in a kinase-independent manner.

The mechanical environment critically regulates cell fate.[2,51] Actin stress fiber formation, a measure of EC contraction, increased upon elevation of substrate stiffness from a physiologically relevant level (8.6 kPa) to a non-physiological level (42 kPa).[52] Similarly, oscillatory but not laminar flow increased EC permeability.[53] We showed that Young's modulus in control ECs is around ~800 Pa and increased significantly in FAK-depleted ECs. Pulmonary ECs show a wide variation in Young's modulus (250–300 Pa to 0.1 Mpa).[54] The values we obtained in the current study using AFM at an indentation rate of 1 m/s fall near the lower limit of the previously reported range.[55] We also showed that FAK depletion increased intracellular tension in ECs due to activating the RhoA pathway, which was conveyed to the nucleus via actomyosin filaments to change EC fate.

FAK is a crucial integrin-linked protein whose kinase activity increases upon phosphorylation at tyrosine residues 397 and 576/577.[7,16,18,56,57] While decreased FAK expression in endothelium causes lung injury,[19,20] increased expression of FAK and activity are seen in several cancers.[58] However, FAK inhibitors employed in cancer studies do not induce lung edema. Our data using the KD-FAK mutant and FAK inhibitor resolved this problem. We showed that FAK functions in a kinase-independent manner to maintain EC stiffness, restrictive fate, and vascular homeostasis in the lungs. We also showed that EC-FAK deletion did not affect vascular homeostasis in other organs, such as the heart, liver, and kidney. ECs constitute about 40%–50% of the lung cell population and are genotypically different in other organs.[59] From these findings, we interpret that FAK regulates cellular signaling context dependently, such as lung injury versus cancer.

FAK orchestrates outside-in signaling by suppressing the RhoA pathway via activation of 190RhoGAP or WASP-ARP2-Rac1 activities.[1,6,8,18,50] FAK can also regulate EC functions, such as proliferation and migration, in a kinase-independent manner.[21] Thus, loss of FAK may increase intracellular tension in a kinase-dependent or -independent manner. We have demonstrated that, in a kinase-independent manner, FAK maintains EC tension by controlling the activation of RhoA, which we proved to be an essential factor in the genesis of the observed phenotypes in FAK-depleted ECs.

Matrix rigidity is known to regulate the transmission of intracellular tension to the nucleus.[60,61] An externally applied mechanical load or fibronectin sensed by integrins at the focal adhesions activates FAK, cSrc, and RhoA signaling.[50] While we did not measure matrix rigidity in FAK-depleted cells, we showed that these cells developed increased

intracellular force, which was transduced to the nucleus via actin stress fibers, leading to emerin phosphorylation and activation of DNMT3a activity via the RhoA-cSrc pathway. Moreover, DNMT activity was increased in ECs plated on a stiff matrix. These findings suggest that FAK controlled tension development and transmission to the nucleus in ECs through guarding matrix rigidity and RhoA-cSrc signaling.

Studies demonstrate that inhibiting FAK activity in smooth muscle cells induces FAK translocation into the nucleus, which regulates DNMT3a activity and the smooth muscle contractile phenotype.[23] While the FAK inhibitor did not affect FAK translocation or DNMT3a activity, the WT- or KD-FAK suppressed DNMT3a activity and rescued the restrictive EC phenotype in FAK-depleted ECs or mice lacking FAK in ECs. Further, suppression of RhoA activity reduced EC tension and DNMT3a activity in FAK-depleted ECs. Similarly, the phospho-deficient emerin mutant or impaired DNMT3a activity rescued tension, EC barrier function, and restrictive EC fate in FAK-depleted cells and lungs. These findings suggest a negative feedback loop formed by FAK in which FAK suppression of RhoA signaling is required to control cell tension and nuclear signaling independently of FAK activity.

Several transcription factors, such as ERG,[62] FoxC,[63] KLF2,[64] and EGR1,[30] are known to be involved in maintaining the barrier-restrictive EC transcriptome. However, our findings identified KLF2 as the tension-sensitive transcription factor using global ATAC-seq analysis. ECs express KLF2 and KLF4 at high levels, which regulate genes crucial for EC adaptation to shear flow and barrier function.[64] We showed that FAK deletion markedly suppresses KLF2 activity but did not affect KLF4 expression. In line with this notion, rescuing KLF2 expression in FAK-depleted ECs or lung vessels restored the restrictive EC phenotype and, thereby, lung homeostasis.

Specific open-chromatin states in regions recognized by epigenetic regulators, including DNA methyltransferases, enable the synthesis of transcription factors driving EC fate during development.[65] Moreover, DNA methylation regulates KLF2 expression.[40] We showed that loss of FAK induced leaky phenotype due to methylation of the KLF2 promoter and reduced *KLF2* synthesis due to activation of DNMT3a. Hence, deleting or inhibiting DNMT3a in ECs of FAK-null mice rescued KLF2 and S1PR1 synthesis and lung vascular homeostasis.

KLF2 regulates several EC genes,[64] but our transcriptome analysis of FAK-null ECs identified S1PR1 as the top hit. *S1PR1* maintains vascular homeostasis basally and reverses vascular barrier function after lung injury.[30] Furthermore, we showed that KLF2 bound the *S1PR1* promoter and increased S1PR1 luciferase activity, which was consistent with previous findings.[66] Thus, transduction of KLF2 in ECs of FAK-null mice restored lung vascular homeostasis. In line with these findings, KLF2 induced S1PR1 expression in response to statins in lung ECs and T cells.[45,67] These findings indicate that inducing KLF2 transcriptional activity can rescue nuclear mechanotransduction and the leaky EC phenotype without FAK.

Phosphorylation of emerin Y74 and Y95 residues by cSrc mediates the mechanical adaptation of nuclei to mechanical force.[47] We showed increased nuclear tension in

FAK-depleted ECs, which was reversed by overexpression of a phosphor-deficient emerin mutant. A possible scenario may be that emerin-mediated nuclear stiffening alters histones, triggering DNMT3a activity.[68] Nevertheless, our findings support recent studies, which suggest that DNMT3a plays a crucial role in suppressing KLF2 expression in ECs under flow conditions.[69] Indeed, we showed that overexpression of phosphor-defective emerin rescued synthesis of the restrictive EC transcriptome and stabilized barrier function in FAK-depleted ECs, thus demonstrating emerin to be the target of FAK and to affect EC fate and hence vascular homeostasis.

In summary, our evidence provides crucial insights into how FAK, in a kinase-independent manner, shapes the EC transcriptome and prevents its conversion to the injury-inducing EC phenotype. ALI and ARDS remain challenging lung diseases despite the emergence of new pharmacological and cell therapies.[3] An important question is whether ECs can be converted from their leaky to restrictive phenotype during injury to promote vascular repair and restore lung homeostasis. We showed that inhibiting emerin phosphorylation or DNMT3a activity enabled KLF2 transcription of *S1PR1* and rescued the EC-restrictive phenotype. These findings suggest that FAK is a potential target for restoring the EC-restrictive phenotype, vascular homeostasis, and tissue function.

Limitations of the study

The study showed that FAK depletion increased nuclear tension via the RhoA-Rho-kinase pathway, which was counteracted by expressing KD-FAK or DN-RhoA mutants. However, how KD-FAK restricted RhoA activity needs to be investigated. We also showed that the Rho-kinase-cSrc pathway increased nuclear tension by phosphorylating emerin. Whether Rho kinase and cSrc translocate to the nucleus to phosphorylate emerin remains to be clarified. Findings also showed that phosphorylated emerin induced DNMT3a activity in the nucleus. DNMT3a exists in dynamic equilibrium between autoinhibitory and active forms. Further analyses are warranted to assess how emerin increased DNMT3a activity. We also demonstrated the therapeutic effectiveness of inhibiting DNMT3a in resolving lung edema in WT mice, but these data do not rule out the contribution of DNMT3a from non-ECs.

STAR★METHODS

RESOURCE AVAILABILITY

Lead contact—Further information and requests for resources and reagents should be directed to and will be fulfilled by the lead contact, Dr. Dolly Mehta (dmehta@uic.edu), upon request.

Materials availability—This study did not generate new unique reagents.

Data and code availability

- RNA-seq and ATAC-seq data have been deposited at GEO and are publicly available. Accession numbers are listed in the key resources table.
- This paper does not report the original code.

- Any additional information required to reanalyze the data reported in this paper is available from the lead contact upon request.

EXPERIMENTAL MODEL AND STUDY PARTICIPANT DETAILS

Cell culture—Human pulmonary arterial endothelial cells (HPAEC) obtained from Lonza Allendale, NJ, USA, were used in all cell studies. Cells were cultured in a humidified atmosphere with 5% CO_2 at 37°C in an EGM-2 medium supplemented with growth factors obtained from Lonza, 10% FBS, and penicillin-streptomycin antibiotics. All studies were conducted on HPAEC that were between passages 4–6.

Animals—Mice were approved by the Institutional Animal Care and Use Committee of the University of Illinois Chicago. Four to five weeks *FAK*$^{fl/fl}$, *EC-FAK*$^{-/-}$, *tdTomato-EC*, and *tdTomato-EC-FAK*$^{-/-}$ mice received tamoxifen (80 mg/kg, i.p.) for five consecutive days followed by a rest of 7 days for drug washout. We generated these mice by crossing *FAK*$^{fl/fl}$ with 5′Endo-SCL-FAK-CreERT/5′Endo-SCL-CreERT/Rosa-Tomato lineage tracing mouse line.[30,36] Tamoxifen (MilliporeSigma) was prepared in corn oil (MilliporeSigma) as described.[30] All experiments were performed on 6–8-week-old mice weighing 20–25 gm. Sex-matched groups of male and female mice were used for these studies. No animals were excluded from the analysis. We calculated the sample size using software G Power (or G Power software) based on the pre-designed effect size between the groups based on Cohen's principles at a power = 0.80 and significance level = 0.05.[30]

METHOD DETAILS

Cell culture and transfection—As described previously, HPAEC were transfected at passages 4–6 using Santa Cruz transfection reagent or Amaxa electroporation.[30] FAK was depleted using siRNA 5′-AAACCAUCUUCAUCUUCCCUU -3′ (Dharmacon Inc) or siFAK-2 (Dharmacon Inc)[19] MISSION shRNA (Sigma-Aldrich, Cat #SHCLND) depletes KLF2. ON-TARGETplus human SOX17 and FOXP1 siRNA were acquired from Dharmacon Inc. Ambion Silencer Pre-designed siRNA was used to deplete DNMT3a. Control siRNA (siCtr) ON-TARGETplus non-targeting pool, Dharmacon Inc, was used in all experiments. For transfection experiments, 50 nM of siRNA (single or double knockdown) was used for 72 h. For dual transfection involving cDNA, EC were first transfected with siRNA for 48 h and then transduced with 1.5 μg of indicated cDNAs for another 24 h. These cDNAs were transduced in depleted cells using FuGENE HD transfection reagent (Promega #E2311).[30]

Atomic force microscopy—As described, Young's modulus (*E*) was assessed by atomic force microscopy.[28] An MFP-3D Bio atomic force microscopy (AFM) (Oxford Instruments Asylum Research, Santa Barbara, CA) and silicon nitride cantilever (MLCT, Bruker) were used to perform mechanical measurements. The AFM was set to operate in force mode, and the piezotransducer (PZT) was established to drive the cantilever to approach, touch, and make a cell indentation. Indentation was performed under contact mode, and the cantilever's spring constant was determined from thermal fluctuations before each experiment. To measure cell stiffness, the AFM force curve, which represents the cell indentation, was fitted in the Hertz model to yield Young's modulus, E (cell stiffness). The software (AR14,

Oxford Instruments Asylum Research) recorded the force curve for each measurement. At least five cells and ten force curves per cell were analyzed for each group.

Confocal imaging—HPAEC were rinsed three times with Ca^{2+} and Mg^{2+} containing PBS and fixed with 2% paraformaldehyde. Cells were then incubated with 5% normal goat serum supplemented with 1% Bovine serum albumin in TBS (0.2M Tris base, 1.5M NaCl) for 2 h at room temperature. After rinsing three times with PBS, cells were incubated with 1:50 anti-VE-cadherin (Santa Cruz) or anti-emerin (Cell Signaling) antibody for 1 h at room temperature, following which cells were rinsed again and incubated with 1:250 dilution of Alexa Fluor 594 secondary Donkey anti-rabbit antibody (Thermo Fisher Scientific) at room temperature for 1h. Isotype control primary antibodies (Thermo Fisher Scientific) were used as a negative control to validate the antibody's specificity and eliminate the background signal. DAPI (1:1000) was used to label nuclei.

Lungs were perfused with phosphate-buffered saline (PBS) and the administration of ice-cold 4% paraformaldehyde (PFA). After 2 h, the lungs were equilibrated overnight with a 30% sucrose solution.[30] Lungs were embedded in an Optimal cutting temperature (OCT) compound and frozen at −20°C, followed by 5 to 8μm thickness sectioning. Antigen retrieval was performed in a citrate-based antigen unmasking solution (Vector Laboratories) following the manufacturer's instructions with a slide immersed in retrieval solution. Blocking was performed using 5% normal goat serum supplemented with 1% Bovine serum albumin in TBS (0.2M Tris base, 1.5M NaCl) for 2 h at room temperature. Lung sections were incubated with indicated primary antibodies with a dilution of 1:50 at 4°C overnight. Sections were washed and incubated with appropriate secondary antibodies at 1:200 dilution at Room temperature for 1 h. Slides were mounted with Prolong Gold antifade reagent (Invitrogen). The images were acquired with an inverted laser-scanning confocal microscope (LSM 880, Carl Zeiss Microscopy) using the Zeiss LSM software. Representative images shown in the figures were selected to match the quantitative analysis most accurately. Regions were assigned randomly to avoid biasing.

Image analysis—ImageJ-NIH was used to design the protocols for quantifying all confocal images using standard methods. An area of uniform size was used in different conditions to quantify fluorescence intensity and gap area between two endothelial cells. Moreover, mean immunostaining intensities (gray values of stained cells in 12-bit Zeiss CZI images) were measured. The grayscale image of immunostained cells was thresholded and converted to a binary mask (thresholding parameters were kept constant through all images). Using ImageJ's Image calculator, the original grayscale image was multiplied with the binary mask, resulting in an image in which all pixel values in the grayscale image defined by the binary mask were considered. For 3D reconstruction (z stack) image analysis, we used Imaris software.

Stochastic optical reconstruction microscopy (STORM)—HPAEC were washed with Ca^{2+} and Mg^{2+} containing PBS (X3), fixed with 4% paraformaldehyde for 10 min at room temperature, and then permeabilized in 0.1% Triton X-100 in PBS for 10 min at room temperature. Cells were stained with an anti-5mC antibody (1:1000 dilution) overnight, followed by a secondary antibody conjugated with fluorescent dyes Alexa Fluor 647 for 2

h at room temperature. STORM images were acquired using buffer A (0.5 mL 1M Tris (pH 8.0), 0.146 g NaCl, 50 mL water) and buffer B (2.5 mL 1M Tris (pH 8.0), 0.029 g NaCl, 5 g Glucose, 47.5 mL water). An imaging buffer (GLOX) was prepared as described.[70] Following the manufacturer's protocol, the images were acquired on a GE OMX-SR Super-Resolution Microscope.

GE's OMX-SR super-resolution microscope was equipped with PCO.edge 5.5 cameras with a camera pixel size of 6.5 μm. Images were captured with a 60X 1.49 NA Plan apo objective. The system's optical configuration included a 1.3× intermediate tube lens. The calculated image pixel size (83.3 nm) was factory-adjusted to 80nm ± 1nm in the OMX-SR system. The proprietary SoftWoRx analysis software uses the "Local maximum factor" to adjust the range of accepted probability values, with larger values leading to more detected fluorophores. We used the factor's default value of 0.01 after we tested a range of local maximum factor values in a data subset and visually inspected the identified localizations. The PSF sigma for far-red fluorophore imaging (em:670nm–684nm) was 137.2 nm measured with the SoftWoRx software. The average FWHM was 323.2 nm. The software program reported localization precision as 13 nm in a typical dataset. In addition, we also calculated lateral localization uncertainty of 25.9 nm, as described.[71]

Collagen gel contraction assay—The cellular contractility of control and FAK-depleted EC was evaluated using the cellular collagen gel contraction assay kit (Cell Biolabs) according to the manufacturer's instructions. Collagen gel working solution prepared on ice was added to the EC suspension in a 4:1 ratio. Five hundred μl of the cell-collagen mixture was added to each well of a 24-well plate and incubated for polymerization for 1 h at 37°C. After gel polymerization, 1 mL of complete medium was added, and the mixture was incubated for three days. The collagen gels were then released from the sides of the culture dishes and imaged to quantify the changes in the size of the collagen gels using ImageJ software.

Fluorescence-activated cell sorting—Lungs were minced and digested with 1 mg/mL collagenase A (Roche) for 30 min at 37°C, after which digested tissue was passed through a 70μm cell strainer to obtain single-cell suspensions. Cells were stained with anti-CD31 and anti-CD45 antibodies, and endothelial cells ($CD45^{-}CD31^{+}dsRed^{+}$) were sorted using the Beckman Coulter cell sorter as described.[30]

ATAC-seq—Flow-sorted cells were washed in cold PBS, and nuclei were isolated with nuclear lysis buffer (10 mM tris, 10 mM NaCl, 3 mM $MgCl_2$, and 0.5% IGEPAL-630) and centrifuged at low speeds. The nuclei were resuspended in 50 μL of transposase reaction mixture (22.5 μL nuclease-free water, 25 μL of TD buffer, and 2.5 μL of TDE1 enzyme, (Illumina). Transposition was carried out at 37°C for 30 min, followed by DNA purification with DNA Clean and Concentrator-5 (Zymo Research) according to the manufacturer's recommendation. Following purification, library fragments were PCR-amplified with Nextera XT v2 adapter primers. Traces were evaluated for quality control of the final library's bioanalyzer. According to the manufacturer's instructions, Illumina sequencing was performed at Northwestern University Genomic Core, Chicago. Raw data have been deposited in the gene expression omnibus archive (accession no. GSE207789).

RNA-seq analysis—Endothelial cells ($CD31^{+}CD45$) were sorted from EC-FAK $^{-/-}$ null and control $FAK^{fl/fl}$ mice. RNA was isolated, and quality control (QC) was performed using a bioanalyzer. RNA-Seq analysis was performed in samples with 7–10 RIN (RNA Integrity Number) at Northwestern University Genomic Core Facility, Chicago. Bioinformatics analysis was performed as described.[30] Raw data have been deposited in the gene expression omnibus archive (accession no. GSE212037).

Quantitative real-time PCR—Total RNA was isolated using Trizol reagent (ThermoFisher Scientific) and quantified using BioDrop DUO+ (Biochrom, UK). RNA (1μg) was reverse transcribed using High-Capacity RNA to cDNA Kit (Applied Biosystems) according to the manufacturer's protocol. The cDNA products were assessed using quantitative Real-Time PCR analysis and Fast SYBR Green Master Mix (Applied Biosystems). Each measurement was duplicated using a CFX384 real-time on Applied Biosystems QuantStudio Real-Time PCR System. The PCR conditions were 95°C for 10 min followed by 40 cycles, 95°C for 15 s, and 60°C for 1 min. The quantitative real-time PCR data were analyzed by the 2-ΔΔCT method. The expression of each gene was normalized to GAPDH. Table 2 provides the list of primers used.

Assessment of lung vascular injury—As described previously, the wet-dry weight ratio was determined to quantify lung vascular injury.[30]

Chromatin immunoprecipitation (*ChIP*) assay—Protein-DNA complex (100–120 μg) was immunoprecipitated with the antibody against MEF2 (Santa Cruz) as described previously.[30] DNA fragments were collected by phenol– chloroform–isoamyl alcohol extraction, followed by ethanol precipitation and then resuspended in 14μL nuclease water for PCR. The promoter region of KLF2 targeted a 152bp fragment and was quantified by Sybr green-based real-time quantitative PCR (Q-PCR) using ViiA7 (Applied Biosystem, Foster City, CA). Normal rabbit IgG was used as negative antibody control, and DNA from the input (20–40 μg protein-DNA complexes) was used as an internal control. Primers used to amplify the MEF2 binding on KLF2 are forward 5′-GCAGTCCGGGCTCCCGCAGTAG-3′; reverse 5′-CTTATAGGCGCGGCAGGCAC-3′.

Genomic DNA isolation and bisulfite sequencing—Genomic DNA was isolated from control or FAK-depleted EC using the Qiagen Genomic DNA Kit (Qiagen). According to the manufacturer's instructions, DNA (200 ng) was processed for bisulfite conversion using the EpiTect Plus Bisulfite Kit (Qiagen). The PCR sequence targeting the KLF2 promoter was performed under the following conditions: denaturation at 98°C for 60 s and 35 cycles each of 98°C for 10 s, 55°C for 30 s, and 72°C for 45 s. The primer is listed in Table 1. The PCR products were subcloned into the pGEM-T (pGEM-T Easy Vector System, Promega) using the manufacturer's protocol, and individual clones were sequenced. The Sanger sequencing was performed at the University of Illinois Genomic Core, UIC. The methylation status of the region was determined and analyzed with QUMA (quantification tool for methylation analysis) (http://quma.cdb.riken.jp/top/quma_main_j.html).[72]

Methylation-specific PCR—Since methylation at CpG sites on the promoter of a gene down-regulates its transcription, we quantified DNA methylation at the promoter region of

KLF2 by bisulfite conversion of the DNA. Bisulfite reaction was performed using EpiTect Plus Lyse All Bisulfite Kit (Qiagen), and after sodium bisulfite conversion, the DNA was applied to an EpiTect spin column and washed to remove traces of sodium bisulfite. The converted DNA was eluted with nuclease-free water. PCR reaction was performed for methylated (M) and un-methylated (U) regions using 2 μL of 5X PCR reaction buffer, 0.2 μM of dNTPs (Promega, Madison, WI), 0.2 mM of each forward and reverse primers, GoTaq DNA polymerase, and 1 μL of converted DNA. The primers for methylated and unmethylated sequences, listed in Table 1, were designed using online MethPrimer.[73] Thermal cycling conditions included 94°C for 5 min, 35 cycles of 94°C for 1 min, 55°C for 30 s, 72°C for 1 min, and final extension at 72°C for 10 min. The PCR products were analyzed on 2% agarose gel, and the intensity of methylated to unmethylated bands was quantified.

DNA agarose gel electrophoresis—Agarose gel (1.5%) was prepared in TAE buffer (40 mM Tris-acetate, 1 mM EDTA) by heating. Ethidium bromide (0.5 μg/mL) was added to the melted gel and cast on the electrophoresis tray. PCR amplified products were loaded on the well along with a 100 base pairs ladder. The gel was visualized under a UV illuminator.

DNA methyltransferase activity measurement—Nuclear fraction was isolated from HPAEC using NE-PER Nuclear and Cytoplasmic Extraction Reagents (Thermofisher Scientific) per the manufacturer's protocol. The nuclear lysates were used to assess the DNMT activity following the manufacturer's method of EpiQuik DNA Methyltransferase Activity Assay Kit (EpiGenTek).

Western blotting—HPAEC were lysed using radioimmunoprecipitation assay buffer (RIPA buffer containing 10 mM Tris-HCl pH 8.0, 1 mM EDTA, 0.5 mM EGTA, 1% Triton X-100, 0.1% sodium deoxycholate, 0.1% SDS, 140 mM NaCl and 1 mM phenylmethylsulfonyl fluoride (PMSF) and western blotted using indicated antibodies as described previously.[30]

Immunoprecipitation—Cells were washed with ice-cold PBS and immediately processed for sub-cellular fractionation as described.[18] Sub-cellular nuclear lysates were incubated with anti-Phospho tyrosine (P99 and P20, 1:250) antibodies overnight, adding agarose beads to pull down the immune complexes.[18] Proteins were separated by SDS-PAGE and immunoblotted using indicated antibodies. Dilution for each primary antibody used in the study was as follows: Emerin (1:1000), Lamin A (1:1000), phosphotyrosine (P99 and P20, 1:250). Membranes were then incubated with respective secondary anti-mouse or anti-rabbit (1:10000) antibodies for 2 h, following which the bands were visualized using an imager or autoradiographic films and chemiluminescent western blotting detection substrate.

Measurement of RhoA activity—HPAEC were transfected with control and FAK siRNAs and, after 48 h, transduced with vector, WT-FAK, and KD-FAK. After 72 h, RhoA activity was measured using a RhoA activation pull-down assay kit (Cytoskeleton Inc.) following the manufacturer's protocol. Western blotting was used to analyze samples using the indicated antibodies as described.[16,19]

Luciferase assay—HPAEC were co-transfected with the control vector as well as wild type-S1PR1 and mutated-S1PR1 luciferase vector for 24 h, and luciferase activity was measured using Promega dual luciferase kit according to the manufacturer's protocol.

***Trans*-endothelial electrical resistance (TEER)—**HPAEC were seeded on gelatin-coated gold-plated eight-well electrodes (8W standard Array; 8W10E+) (Applied Biosciences, Carlsbad, CA). Cells were transfected with indicated siRNAs for 48 h. The smaller and larger counter electrodes were connected to a phase-sensitive lock-in amplifier to monitor the voltage. A constant current of 1 μA was supplied by a 1 V, 4000 Hz AC signal connected serially to a 1 MΩ resistor between the smaller electrode and the larger counter electrode. EC monolayers were incubated in a serum-free medium for 2 h, following which S1P was added to assess dynamic change in TEER.[30]

Liposome-mediated in-vivo gene delivery—Liposomes were prepared using a mixture of chloroform, Dimethyl Dioctadecyl Ammonium Bromide, and cholesterol, as described previously.[37] Briefly, chloroform was evaporated from the mixture using a rotavapor system at 105 rpm for 15–20 min at 37°C to make a lipid layer. The lipid layer was extracted by sonicating the solution for 1 h at 42°C in the presence of 5% glucose. The liposomes were filtered through a 0.45-μmmicron filter, and cDNA was subsequently added. The cDNA-loaded liposomes were administered i.v into the mouse. The lungs were harvested for edema measurement after 24 h.

Polyethylene glycol hydrogel preparation—The soft and stiff hydrogels were formulated as described.[39] Briefly, these hydrogels were prepared under exposure to ultraviolet light (365 nm) by adding varying concentrations of lithium phenyl(2,4,6-trimethylbenzoyl) phosphinate (TCI Chemicals) to the solution of PEG-DA Mn 700, 10 mM sodium L-ascorbate, 4 mM tris(2-carboxyethyl) phosphine, 1× phosphate-buffered saline. Cys-RGD peptide (sequence CGGGGRGDSP) at a concentration of 0.16 mM was added to the pre-hydrogel solution to attach the endothelial cells. The increased amount of LAP promotes to achieve improved mechanical strength in terms of Young's modulus.

Statistical analysis—Data are presented as the mean ± SEM. Data were tested for normality and equal variance to confirm the appropriateness of parametric tests. Wherever only two groups were compared, statistical differences were assessed using an unpaired two-tailed Student's t-test. Statistical significance among three groups or over was determined using one-way analysis of variance (ANOVA) followed by post hoc Tukey's multiple comparisons test. The data were analyzed using GraphPad Prism version 8.0, and $p < 0.05$ indicates a statistically significant difference.

Supplementary Material

Refer to Web version on PubMed Central for supplementary material.

ACKNOWLEDGMENTS

This work was supported by the National Institutes of Health, USA grants HL084153, PO1-HL151327, PO1-HL160469, and RO1-HL165263. M.Z.A. was endorsed by the American Heart Association Postdoctoral Fellowship

(AHA award 19POST34450241). We thank Drs. Christophe Guilluy (Institute for Advanced Biosciences, Centre de recherche UGA–INSERM, France) for generously providing WT and phosphodeficient emerin cDNAs, Andrei Karginov (University of Illinois, Chicago, USA) for supplying WT-FAK and KD-FAK cDNAs, Jalees Rehman for SOX17 cDNA, and Hua Yu (Beckman Research Institute and City of Hope Comprehensive Cancer Center, Duarte, CA, USA) for luciferase S1PR1 promoter. We want to acknowledge Lakshmi Yalagala for the skillful performance of the mouse genotyping. The graphical abstract was designed and created using BioRender.com.

REFERENCES

1. Mehta D, and Malik AB (2006). Signaling mechanisms regulating endothelial permeability. Physiol. Rev. 86, 279–367. [PubMed: 16371600]
2. Wang N, Tytell JD, and Ingber DE (2009). Mechanotransduction at a distance: mechanically coupling the extracellular matrix with the nucleus. Nat. Rev. Mol. Cell Biol. 10, 75–82. [PubMed: 19197334]
3. Matthay MA, and Zemans RL (2011). The acute respiratory distress syndrome: pathogenesis and treatment. Annu. Rev. Pathol. 6, 147–163. [PubMed: 20936936]
4. Hariri L, and Hardin CC (2020). Covid-19, Angiogenesis, and ARDS Endotypes. N. Engl. J. Med. 383, 182–183. [PubMed: 32437597]
5. Owen JD, Ruest PJ, Fry DW, and Hanks SK (1999). Induced focal adhesion kinase (FAK) expression in FAK-null cells enhances cell spreading and migration requiring both auto- and activation loop phosphorylation sites and inhibits adhesion-dependent tyrosine phosphorylation of Pyk2. Mol. Cell Biol. 19, 4806–4818. [PubMed: 10373530]
6. Parsons JT (2003). Focal adhesion kinase: the first ten years. J. Cell Sci. 116, 1409–1416. [PubMed: 12640026]
7. Schaller MD (2010). Cellular functions of FAK kinases: insight into molecular mechanisms and novel functions. J. Cell Sci. 123, 1007–1013. [PubMed: 20332118]
8. Braren R, Hu H, Kim YH, Beggs HE, Reichardt LF, and Wang R (2006). Endothelial FAK is essential for vascular network stability, cell survival, and lamellipodial formation. J. Cell Biol. 172, 151–162. [PubMed: 16391003]
9. Dunty JM, Gabarra-Niecko V, King ML, Ceccarelli DFJ, Eck MJ, and Schaller MD (2004). FERM domain interaction promotes FAK signaling. Mol. Cell Biol. 24, 5353–5368. [PubMed: 15169899]
10. Mitra SK, Hanson DA, and Schlaepfer DD (2005). Focal adhesion kinase: in command and control of cell motility. Nat. Rev. Mol. Cell Biol. 6, 56–68. [PubMed: 15688067]
11. Chuang HH, Zhen YY, Tsai YC, Chuang CH, Hsiao M, Huang MS, and Yang CJ (2022). FAK in Cancer: From Mechanisms to Therapeutic Strategies. Int. J. Mol. Sci. 23, 1726. [PubMed: 35163650]
12. Wang HB, Dembo M, Hanks SK, and Wang Y (2001). Focal adhesion kinase is involved in mechanosensing during fibroblast migration. Proc. Natl. Acad. Sci. USA 98, 11295–11300. [PubMed: 11572981]
13. Zhao XK, Cheng Y, Liang Cheng M, Yu L, Mu M, Li H, Liu Y, Zhang B, Yao Y, Guo H, et al. (2016). Focal Adhesion Kinase Regulates Fibroblast Migration via Integrin beta-1 and Plays a Central Role in Fibrosis. Sci. Rep. 6, 19276. [PubMed: 26763945]
14. Taufalele PV, Wang W, Simmons AJ, Southard-Smith AN, Chen B, Greenlee JD, King MR, Lau KS, Hassane DC, Bordeleau F, and Reinhart-King CA (2023). Matrix stiffness enhances cancer-macrophage interactions and M2-like macrophage accumulation in the breast tumor microenvironment. Acta Biomater. 163, 365–377. [PubMed: 35483629]
15. Zaghdoudi S, Decaup E, Belhabib I, Samain R, Cassant-Sourdy S, Rochotte J, Brunel A, Schlaepfer D, Cros J, Neuzillet C, et al. (2020). FAK activity in cancer-associated fibroblasts is a prognostic marker and a druggable key metastatic player in pancreatic cancer. EMBO Mol. Med. 12, e12010. [PubMed: 33025708]
16. Holinstat M, Knezevic N, Broman M, Samarel AM, Malik AB, and Mehta D (2006). Suppression of RhoA activity by focal adhesion kinase-induced activation of p190RhoGAP: role in regulation of endothelial permeability. J. Biol. Chem. 281, 2296–2305. [PubMed: 16308318]

17. Knezevic N, Tauseef M, Thennes T, and Mehta D (2009). The G protein betagamma subunit mediates reannealing of adherens junctions to reverse endothelial permeability increase by thrombin. J. Exp. Med. 206, 2761–2777. [PubMed: 19917775]

18. Rajput C, Kini V, Smith M, Yazbeck P, Chavez A, Schmidt T, Zhang W, Knezevic N, Komarova Y, and Mehta D (2013). Neural Wiskott-Aldrich syndrome protein (N-WASP)-mediated p120-catenin interaction with Arp2-Actin complex stabilizes endothelial adherens junctions. J. Biol. Chem. 288, 4241–4250. [PubMed: 23212915]

19. Schmidt TT, Tauseef M, Yue L, Bonini MG, Gothert J, Shen TL, Guan JL, Predescu S, Sadikot R, and Mehta D (2013). Conditional deletion of FAK in mice endothelium disrupts lung vascular barrier function due to destabilization of RhoA and Rac1 activities. Am. J. Physiol. Lung Cell Mol. Physiol. 305, L291–L300. [PubMed: 23771883]

20. Ying L, Alvira CM, and Cornfield DN (2018). Developmental differences in focal adhesion kinase expression modulate pulmonary endothelial barrier function in response to inflammation. Am. J. Physiol. Lung Cell Mol. Physiol. 315, L66–L77. [PubMed: 29597831]

21. Zhao X, Peng X, Sun S, Park AYJ, and Guan JL (2010). Role of kinase-independent and -dependent functions of FAK in endothelial cell survival and barrier function during embryonic development. J. Cell Biol. 189, 955–965. [PubMed: 20530207]

22. Shen TL, Park AYJ, Alcaraz A, Peng X, Jang I, Koni P, Flavell RA, Gu H, and Guan JL (2005). Conditional knockout of focal adhesion kinase in endothelial cells reveals its role in angiogenesis and vascular development in late embryogenesis. J. Cell Biol. 169, 941–952. [PubMed: 15967814]

23. Jeong K, Murphy JM, Kim JH, Campbell PM, Park H, Rodriguez YAR, Choi CS, Kim JS, Park S, Kim HJ, et al. (2021). FAK Activation Promotes SMC Dedifferentiation via Increased DNA Methylation in Contractile Genes. Circ. Res. 129, e215–e233. [PubMed: 34702049]

24. Murphy JM, Jeong K, Cioffi DL, Campbell PM, Jo H, Ahn EYE, and Lim STS (2021). Focal Adhesion Kinase Activity and Localization is Critical for TNF-α-Induced Nuclear Factor-κB Activation. Inflammation 44, 1130–1144. [PubMed: 33527321]

25. Zhou J, Aponte-Santamaría C, Sturm S, Bullerjahn JT, Bronowska A, and Gräter F (2015). Mechanism of Focal Adhesion Kinase Mechanosensing. PLoS Comput. Biol. 11, e1004593. [PubMed: 26544178]

26. Zhou DW, Fernández-Yagüe MA, Holland EN, García AF, Castro NS, O'Neill EB, Eyckmans J, Chen CS, Fu J, Schlaepfer DD, and García AJ (2021). Force-FAK signaling coupling at individual focal adhesions coordinates mechanosensing and microtissue repair. Nat. Commun. 12, 2359. [PubMed: 33883558]

27. Bastounis EE, Yeh YT, and Theriot JA (2019). Subendothelial stiffness alters endothelial cell traction force generation while exerting a minimal effect on the transcriptome. Sci. Rep. 9, 18209. [PubMed: 31796790]

28. Wong SW, Lenzini S, Bargi R, Feng Z, Macaraniag C, Lee JC, Peng Z, and Shin JW (2020). Controlled Deposition of 3D Matrices to Direct Single Cell Functions. Adv. Sci. 7, 2001066.

29. Discher DE, Janmey P, and Wang YL (2005). Tissue cells feel and respond to the stiffness of their substrate. Science 310, 1139–1143. [PubMed: 16293750]

30. Akhter MZ, Chandra Joshi J, Balaji Ragunathrao VA, Maienschein-Cline M, Proia RL, Malik AB, and Mehta D (2021). Programming to S1PR1(+) Endothelial Cells Promotes Restoration of Vascular Integrity. Circ. Res. 129, 221–236. [PubMed: 33926208]

31. Kimura K, Ito M, Amano M, Chihara K, Fukata Y, Nakafuku M, Yamamori B, Feng J, Nakano T, Okawa K, et al. (1996). Regulation of myosin phosphatase by Rho and Rho-associated kinase (Rho-kinase). Science 273, 245–248. [PubMed: 8662509]

32. Mehta D, Tiruppathi C, Sandoval R, Minshall RD, Holinstat M, and Malik AB (2002). Modulatory role of focal adhesion kinase in regulating human pulmonary arterial endothelial barrier function. J. Physiol. 539, 779–789. [PubMed: 11897849]

33. Even-Ram S, Doyle AD, Conti MA, Matsumoto K, Adelstein RS, and Yamada KM (2007). Myosin IIA regulates cell motility and actomyosin-microtubule crosstalk. Nat. Cell Biol. 9, 299–309. [PubMed: 17310241]

34. Watanabe K, Ueno M, Kamiya D, Nishiyama A, Matsumura M, Wataya T, Takahashi JB, Nishikawa S, Nishikawa SI, Muguruma K, and Sasai Y (2007). A ROCK inhibitor permits survival of dissociated human embryonic stem cells. Nat. Biotechnol. 25, 681–686. [PubMed: 17529971]
35. Alexopoulou AN, Lees DM, Bodrug N, Lechertier T, Fernandez I, D'Amico G, Dukinfield M, Batista S, Tavora B, Serrels B, and Hodivala-Dilke K (2017). Focal Adhesion Kinase (FAK) tyrosine 397E mutation restores the vascular leakage defect in endothelium-specific FAK-kinase dead mice. J. Pathol. 242, 358–370. [PubMed: 28444899]
36. Liu M, Zhang L, Marsboom G, Jambusaria A, Xiong S, Toth PT, Benevolenskaya EV, Rehman J, and Malik AB (2019). Sox17 is required for endothelial regeneration following inflammation-induced vascular injury. Nat. Commun. 10, 2126. [PubMed: 31073164]
37. Tauseef M, Knezevic N, Chava KR, Smith M, Sukriti S, Gianaris N, Obukhov AG, Vogel SM, Schraufnagel DE, Dietrich A, et al. (2012). TLR4 activation of TRPC6-dependent calcium signaling mediates endotoxin-induced lung vascular permeability and inflammation. J. Exp. Med. 209, 1953–1968. [PubMed: 23045603]
38. Uhler C, and Shivashankar GV (2017). Regulation of genome organization and gene expression by nuclear mechanotransduction. Nat. Rev. Mol. Cell Biol. 18, 717–727. [PubMed: 29044247]
39. Lenzini S, Debnath K, Joshi JC, Wong SW, Srivastava K, Geng X, Cho IS, Song A, Bargi R, Lee JC, et al. (2021). Cell-Matrix Interactions Regulate Functional Extracellular Vesicle Secretion from Mesenchymal Stromal Cells. ACS Nano 15, 17439–17452. [PubMed: 34677951]
40. Kumar A, Kumar S, Vikram A, Hoffman TA, Naqvi A, Lewarchik CM, Kim YR, and Irani K (2013). Histone and DNA methylation-mediated epigenetic downregulation of endothelial Kruppel-like factor 2 by low-density lipoprotein cholesterol. Arterioscler. Thromb. Vasc. Biol. 33, 1936–1942. [PubMed: 23723375]
41. Li Y, and Tollefsbol TO (2011). DNA methylation detection: bisulfite genomic sequencing analysis. Methods Mol. Biol. 791, 11–21. [PubMed: 21913068]
42. Denis H, Ndlovu MN, and Fuks F (2011). Regulation of mammalian DNA methyltransferases: a route to new mechanisms. EMBO Rep. 12, 647–656. [PubMed: 21660058]
43. Tauseef M, Kini V, Knezevic N, Brannan M, Ramchandaran R, Fyrst H, Saba J, Vogel SM, Malik AB, and Mehta D (2008). Activation of sphingosine kinase-1 reverses the increase in lung vascular permeability through sphingosine-1-phosphate receptor signaling in endothelial cells. Circ. Res. 103, 1164–1172. [PubMed: 18849324]
44. Garcia JG, Liu F, Verin AD, Birukova A, Dechert MA, Gerthoffer WT, Bamberg JR, and English D (2001). Sphingosine 1-phosphate promotes endothelial cell barrier integrity by Edg-dependent cytoskeletal rearrangement. J. Clin. Invest. 108, 689–701. [PubMed: 11544274]
45. Skon CN, Lee JY, Anderson KG, Masopust D, Hogquist KA, and Jameson SC (2013). Transcriptional downregulation of S1pr1 is required for the establishment of resident memory CD8+ T cells. Nat. Immunol. 14, 1285–1293. [PubMed: 24162775]
46. Tifft KE, Bradbury KA, and Wilson KL (2009). Tyrosine phosphorylation of nuclear-membrane protein emerin by Src, Abl and other kinases. J. Cell Sci. 122, 3780–3790. [PubMed: 19789182]
47. Guilluy C, Osborne LD, Van Landeghem L, Sharek L, Superfine R, Garcia-Mata R, and Burridge K (2014). Isolated nuclei adapt to force and reveal a mechanotransduction pathway in the nucleus. Nat. Cell Biol. 16, 376–381. [PubMed: 24609268]
48. Sieg DJ, Ilić D, Jones KC, Damsky CH, Hunter T, and Schlaepfer DD (1998). Pyk2 and Src-family protein-tyrosine kinases compensate for the loss of FAK in fibronectin-stimulated signaling events but Pyk2 does not fully function to enhance FAK- cell migration. EMBO J. 17, 5933–5947. [PubMed: 9774338]
49. Higuchi M, Ishiyama K, Maruoka M, Kanamori R, Takaori-Kondo A, and Watanabe N (2021). Paradoxical activation of c-Src as a drug-resistant mechanism. Cell Rep. 34, 108876. [PubMed: 33761359]
50. Li S, Butler P, Wang Y, Hu Y, Han DC, Usami S, Guan JL, and Chien S (2002). The role of the dynamics of focal adhesion kinase in the mechanotaxis of endothelial cells. Proc. Natl. Acad. Sci. USA 99, 3546–3551. [PubMed: 11891289]
51. Ingber DE (2002). Mechanical signaling and the cellular response to extracellular matrix in angiogenesis and cardiovascular physiology. Circ. Res. 91, 877–887. [PubMed: 12433832]

52. Birukova AA, Tian X, Cokic I, Beckham Y, Gardel ML, and Birukov KG (2013). Endothelial barrier disruption and recovery is controlled by substrate stiffness. Microvasc. Res. 87, 50–57. [PubMed: 23296034]
53. Sei YJ, Ahn SI, Virtue T, Kim T, and Kim Y (2017). Detection of frequency-dependent endothelial response to oscillatory shear stress using a microfluidic transcellular monitor. Sci. Rep. 7, 10019. [PubMed: 28855638]
54. Birukova AA, Arce FT, Moldobaeva N, Dudek SM, Garcia JGN, Lal R, and Birukov KG (2009). Endothelial permeability is controlled by spatially defined cytoskeletal mechanics: atomic force microscopy force mapping of pulmonary endothelial monolayer. Nanomedicine 5, 30–41. [PubMed: 18824415]
55. Delgadillo LF, Marsh GA, and Waugh RE (2020). Endothelial Glycocalyx Layer Properties and Its Ability to Limit Leukocyte Adhesion. Biophys. J. 118, 1564–1575. [PubMed: 32135082]
56. Frame MC, Patel H, Serrels B, Lietha D, and Eck MJ (2010). The FERM domain: organizing the structure and function of FAK. Nat. Rev. Mol. Cell Biol. 11, 802–814. [PubMed: 20966971]
57. Lietha D, Cai X, Ceccarelli DFJ, Li Y, Schaller MD, and Eck MJ (2007). Structural basis for the autoinhibition of focal adhesion kinase. Cell 129, 1177–1187. [PubMed: 17574028]
58. Roy-Luzarraga M, and Hodivala-Dilke K (2016). Molecular Pathways: Endothelial Cell FAK-A Target for Cancer Treatment. Clin. Cancer Res. 22, 3718–3724. [PubMed: 27262114]
59. Jambusaria A, Hong Z, Zhang L, Srivastava S, Jana A, Toth PT, Dai Y, Malik AB, and Rehman J (2020). Endothelial heterogeneity across distinct vascular beds during homeostasis and inflammation. Elife 9, e51413. [PubMed: 31944177]
60. Hoffman BD, Grashoff C, and Schwartz MA (2011). Dynamic molecular processes mediate cellular mechanotransduction. Nature 475, 316–323. [PubMed: 21776077]
61. Guilluy C, and Burridge K (2015). Nuclear mechanotransduction: forcing the nucleus to respond. Nucleus 6, 19–22. [PubMed: 25738642]
62. Lathen C, Zhang Y, Chow J, Singh M, Lin G, Nigam V, Ashraf YA, Yuan JX, Robbins IM, and Thistlethwaite PA (2014). ERG-APLNR axis controls pulmonary venule endothelial proliferation in pulmonary veno-occlusive disease. Circulation 130, 1179–1191. [PubMed: 25062690]
63. Xia S, Yu W, Menden H, Younger ST, and Sampath V (2021). FOXC2 Autoregulates Its Expression in the Pulmonary Endothelium After Endotoxin Stimulation in a Histone Acetylation-Dependent Manner. Front. Cell Dev. Biol. 9, 657662. [PubMed: 34017833]
64. Atkins GB, and Jain MK (2007). Role of Krüppel-like transcription factors in endothelial biology. Circ. Res. 100, 1686–1695. [PubMed: 17585076]
65. Russell-Hallinan A, Watson CJ, O'Dwyer D, Grieve DJ, and O'Neill KM (2021). Epigenetic Regulation of Endothelial Cell Function by Nucleic Acid Methylation in Cardiac Homeostasis and Disease. Cardiovasc. Drugs Ther. 35, 1025–1044.
66. Sun X, Mathew B, Sammani S, Jacobson JR, and Garcia JGN (2017). Simvastatin-induced sphingosine 1-phosphate receptor 1 expression is KLF2-dependent in human lung endothelial cells. Pulm. Circ. 7, 117–125. [PubMed: 28680571]
67. Bu DX, Tarrio M, Grabie N, Zhang Y, Yamazaki H, Stavrakis G, Maganto-Garcia E, Pepper-Cunningham Z, Jarolim P, Aikawa M, et al. (2010). Statin-induced Krüppel-like factor 2 expression in huma n and mouse T cells reduces inflammatory and pathogenic responses. J. Clin. Invest. 120, 1961–1970. [PubMed: 20440076]
68. Guo X, Wang L, Li J, Ding Z, Xiao J, Yin X, He S, Shi P, Dong L, Li G, et al. (2015). Structural insight into autoinhibition and histone H3-induced activation of DNMT3A. Nature 517, 640–644. [PubMed: 25383530]
69. Parmar KM, Larman HB, Dai G, Zhang Y, Wang ET, Moorthy SN, Kratz JR, Lin Z, Jain MK, Gimbrone MA Jr., and García-Cardeña G (2006). Integration of flow-dependent endothelial phenotypes by Kruppel-like factor 2. J. Clin. Invest. 116, 49–58. [PubMed: 16341264]
70. Xu J, Ma H, and Liu Y (2017). Stochastic Optical Reconstruction Microscopy (STORM). Curr. Protoc. Cytom. 81, 12.46.11–12.46.27.
71. Rieger B, and Stallinga S (2014). The lateral and axial localization uncertainty in super-resolution light microscopy. ChemPhysChem 15, 664–670. [PubMed: 24302478]

72. Kumaki Y, Oda M, and Okano M (2008). QUMA: quantification tool for methylation analysis. Nucleic Acids Res. 36, W170–W175. [PubMed: 18487274]

73. Li LC, and Dahiya R (2002). MethPrimer: designing primers for methylation PCRs. Bioinformatics 18, 1427–1431. [PubMed: 12424112]

Highlights

- FAK, in a kinase-independent manner, safeguards tension transmission to the nucleus
- Loss of endothelial FAK induces RhoA pathway activating nuclear emerin and DNMT3a
- Suppression of KLF2 by DNMT3a subverts EC transcriptome to leaky phenotype
- Restoring FAK or inhibiting DNMT3a rescues KLF2 transcription of restricted EC

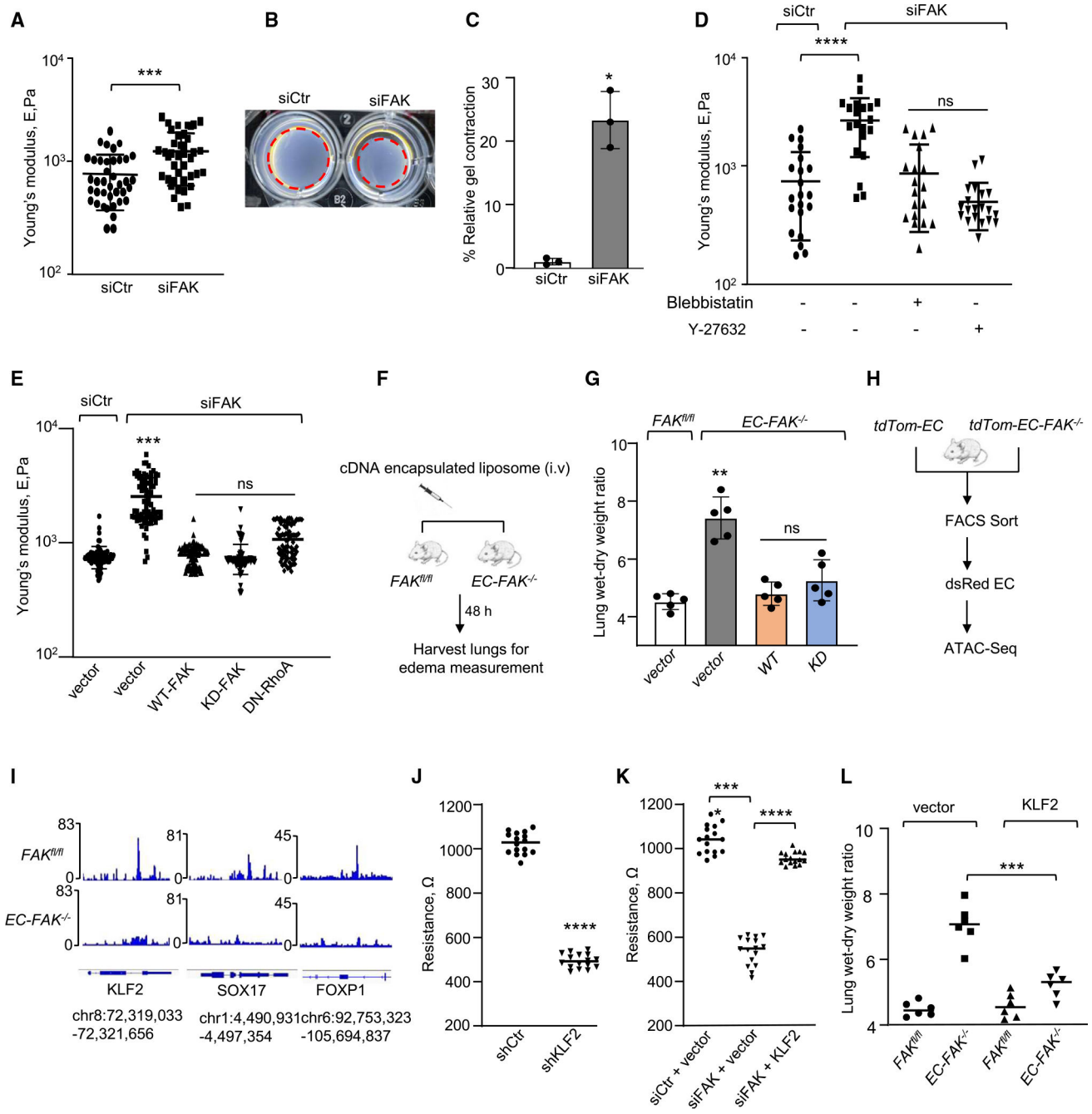

Figure 1. FAK regulation of nuclear mechanotransduction controls chromatin accessibility of transcription factors

(A) Young's modulus (*E*) in a single control or FAK-depleted ECs using atomic force microscopy (AFM) by nanoscale indentation at 1 m/s. $N = 40$ cells/group, pooled from three independent experiments ($n = 3$, unpaired t test).

(B and C) Collagen gel contraction assay in control and FAK-depleted ECs. A representative photograph is shown in (B), while (C) shows the quantification of gel contraction from three independent experiments ($n = 3$, unpaired t test).

(D) Young's modulus (E) in FAK-depleted ECs following 1-h treatment with 20 μM blebbistatin or 10 μM Y-27632. The data were pooled from three independent experiments (one-way ANOVA with Tukey's *post hoc* test).

(E) Young's modulus in FAK-depleted EC transducing vector, WT-FAK, KD-FAK, and DN-RhoA cDNAs performed as in (A). $N = 40$ cells/group, pooled from three independent experiments ($n = 3$, one-way ANOVA with Tukey's *post hoc* test).

(F and G) Workflow of indicated cDNAs delivery in ECs of EC-FAK-null and control mice using liposomes (F) and lung edema (G) assessment ($n = 5$ mice/group, one-way ANOVA with Tukey's *post hoc* test).

(H and I) Schematic of EC sorting ($CD45^{-}CD31^{+}dsRed^{+}$) from lungs of control tdTomato and tdTomato-EC-$FAK^{-/-}$ mice for ATAC-seq analysis (H). Snapshot of genomic loci obtained from Integrative Genomic Viewer, showing chromatin-accessible peaks at the transcription start sites (TSSs) for KLF2, SOX17, and FOXP1 in $FAK^{fl/fl}$ and EC-$FAK^{/}$lung ECs (I).

(J and K) TEER in control (sh), KLF2-depleted ECs (shKLF2) (J), or FAK-depleted EC transducing vector or KLF2 cDNA (K). The data were pooled from four experiments ($n = 4$ wells/group) (unpaired t test for J, one-way ANOVA with Tukey's *post hoc* test for K).

(L) Lung edema in control or EC-FAK-null mice following indicated gene delivery as described in (F) and (G) ($n = 6$ mice/group, one-way ANOVA with Tukey's *post hoc* test).

Data show individual values along with mean ± SEM. Statistical significance: $*p < 0.05$, $**p < 0.01$, $***p < 0.001$, $****p < 0.0001$; ns, not significant. Please see Figure S1.

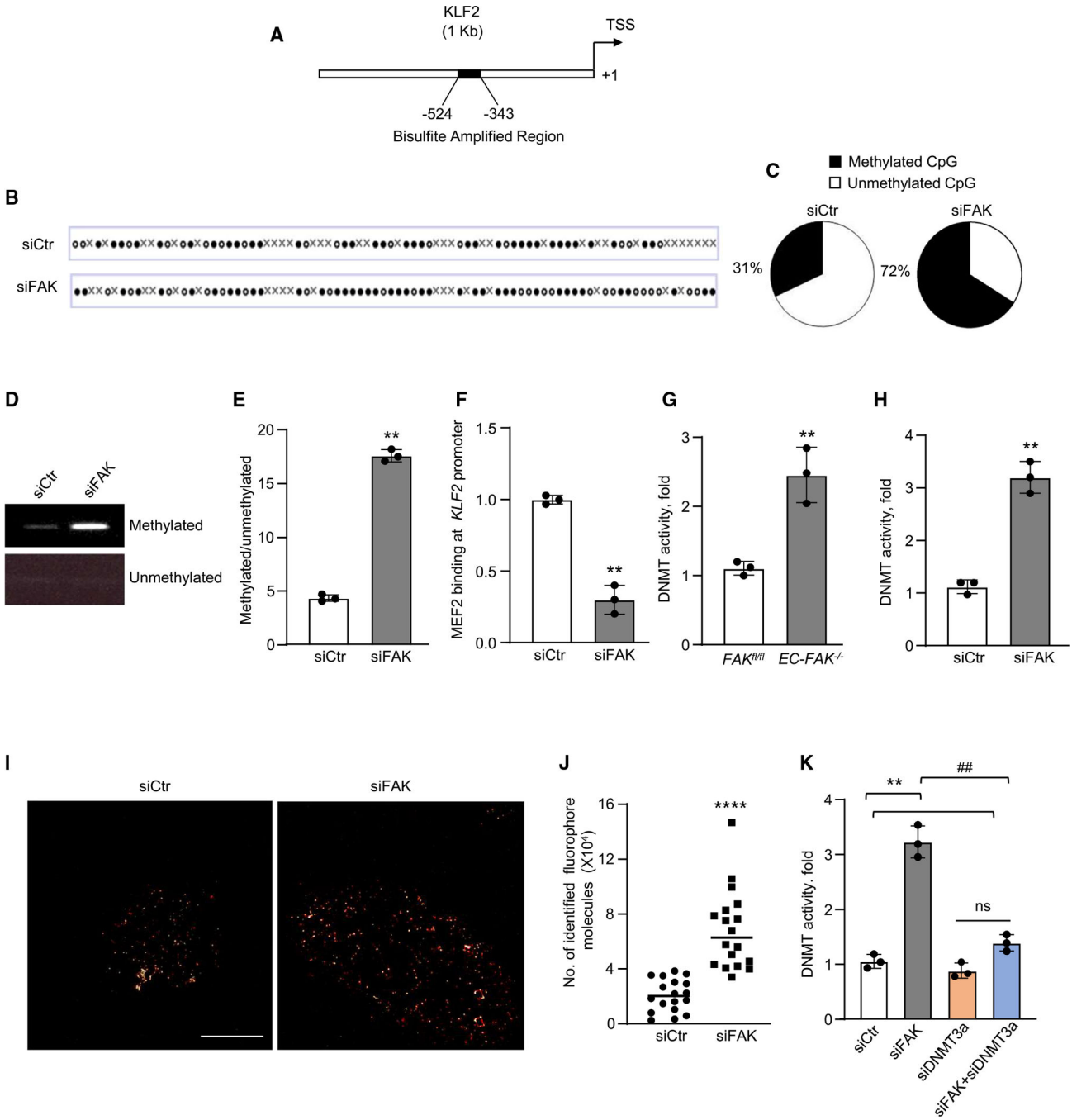

Figure 2. FAK upregulates KLF2 by suppressing DNA methylation of *KLF2* promoter

(A) Schematic of *KLF2* promoter containing CpG island (−343 to −524) from the transcription start site.

(B and C) (B) Bisulfite sequencing of whole-genome DNA from control or FAK-depleted ECs to quantify *KLF2* promoter methylation using quantification tool for methylation analysis (QUMA). Methylated CpG, dark circles; unmethylated CpG, clear circles. (C) A pie-chart of quantified methylated and unmethylated CpG ($n = 3$).

(D and E) Methylation-specific PCR (MS-PCR) of bisulfite-converted genomic DNA from control or FAK-depleted ECs. A representative DNA agarose gel of amplified products is shown in (D), while (E) shows the quantification of the amplified products ($n = 3$, unpaired t test).

(F) Chromatin immunoprecipitation (ChIP) assay followed by qPCR of amplified MEF2 binding on *KLF2* promoter in control or FAK-depleted ECs ($n = 3$, unpaired t test).

(G and H) DNMT activity in $FAK^{fl/fl}$ and $EC\text{-}FAK^{-/-}$ lungs (G) or control and FAK-depleted ECs (H) ($n = 3$, unpaired t test).

(I and J) Stochastic optical reconstruction microscopy (STORM) imaging of single nuclei in control versus FAK-depleted ECs performed using GE OMX-SR Super-Resolution microscope. A representative micrograph is shown in (I), while (J) shows the quantification of 5-mC fluorophore molecules in 18 nuclei from control or FAK-depleted ECs pooled from three independent experiments ($n = 3$, unpaired t test). Scale bar: 5 μm.

(K) DNMT activity in control, FAK-depleted, DNMT3a-depleted, and DNMT3a- and FAK-depleted ECs (n = 3; one-way ANOVA with Tukey's *post hoc* test).

Data show individual values with mean ± SEM. Statistical significance: $^{**}p < 0.01$, $^{\#\#}p < 0.01$, $^{****}p < 0.0001$; ns, not significant.

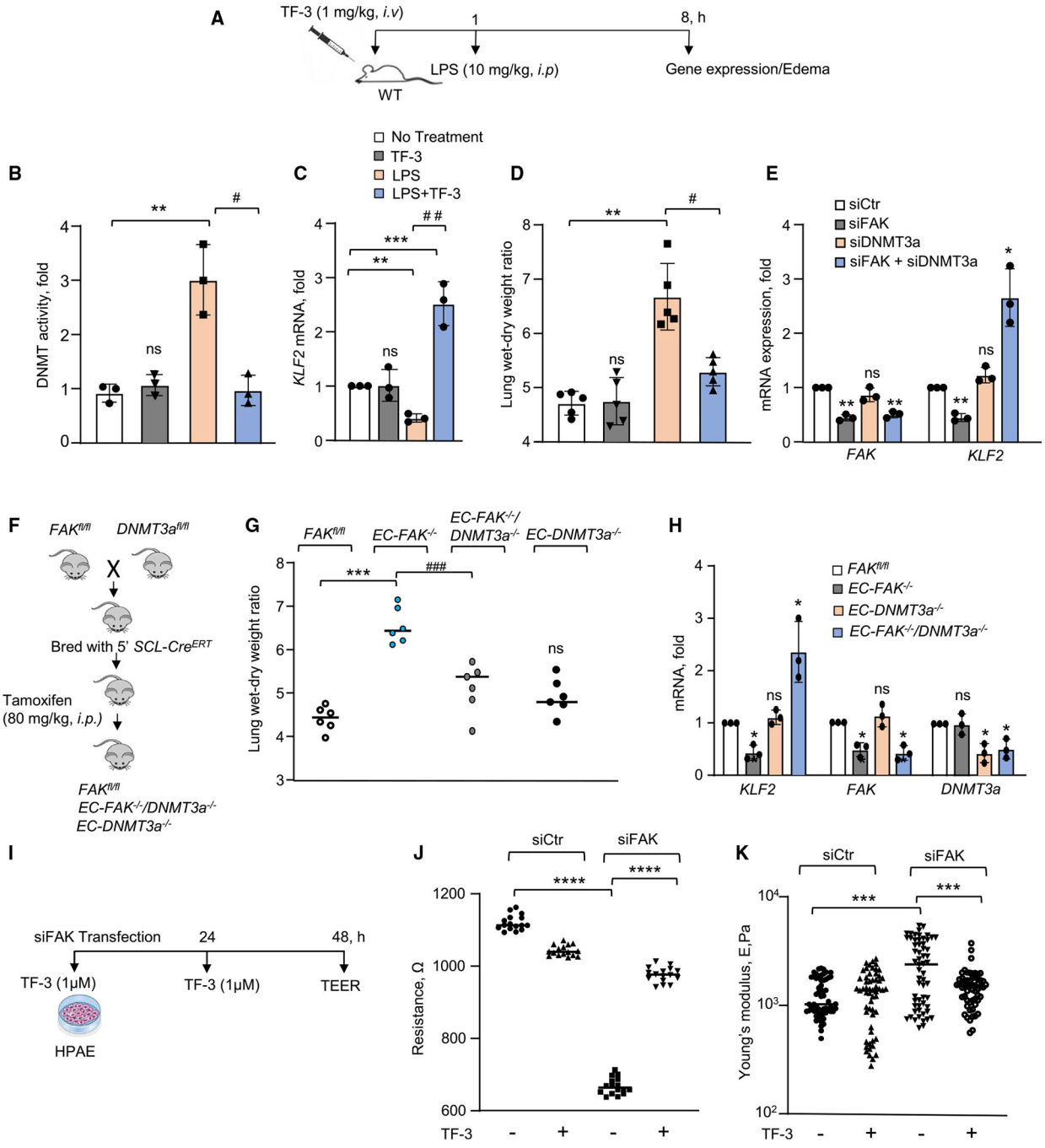

Figure 3. DNMT3a compromises lung vascular homeostasis in FAK-deleted ECs

(A–D) Protocol for inhibiting DNMT3a in lungs of WT mice (A) and assessment of DNMT activity ($n = 3$) (B), lung *KLF2* mRNA expression ($n = 3$) (C), and lung edema ($n = 5$ mice/group) (D) (one-way ANOVA with Tukey's *post hoc* test).

(E) *FAK* and *KLF2* mRNA expression in control, FAK-depleted, DNMT3a, and FAK+DNMT3a-depleted ECs using GAPDH as an internal control ($n = 3$, one-way ANOVA with Tukey's *post hoc* test).

(F–H) Schematic of *EC-FAK*$^{-/-}$/*DNMT3a*$^{-/-}$ (double knockout) mouse generation (F). (G) Lung edema in the indicated mouse group (n = 6 mice/group, one-way ANOVA with Tukey's *post hoc test*). (H) mRNA expression of indicated genes using GAPDH as an internal control (n = 3, one-way ANOVA with Tukey's *post hoc* test).

(I–K) Schematic for theaflavin-3,3′-digallate (TF-3) treatment (I), TEER (J), and Young's modulus (K). The data were pooled from four experiments (n = 4 wells/group), and N = 40 cells/group in (K) pooled from three independent experiments (one-way ANOVA with Tukey's *post hoc* test in J and K).

Data show scatter along with mean ± SEM. Statistical significance: *p < 0.05, #p < 0.05, **p < 0.01, ##p < 0.01, ***p < 0.001, ###p < 0.001, ****p < 0.0001; ns, not significant.

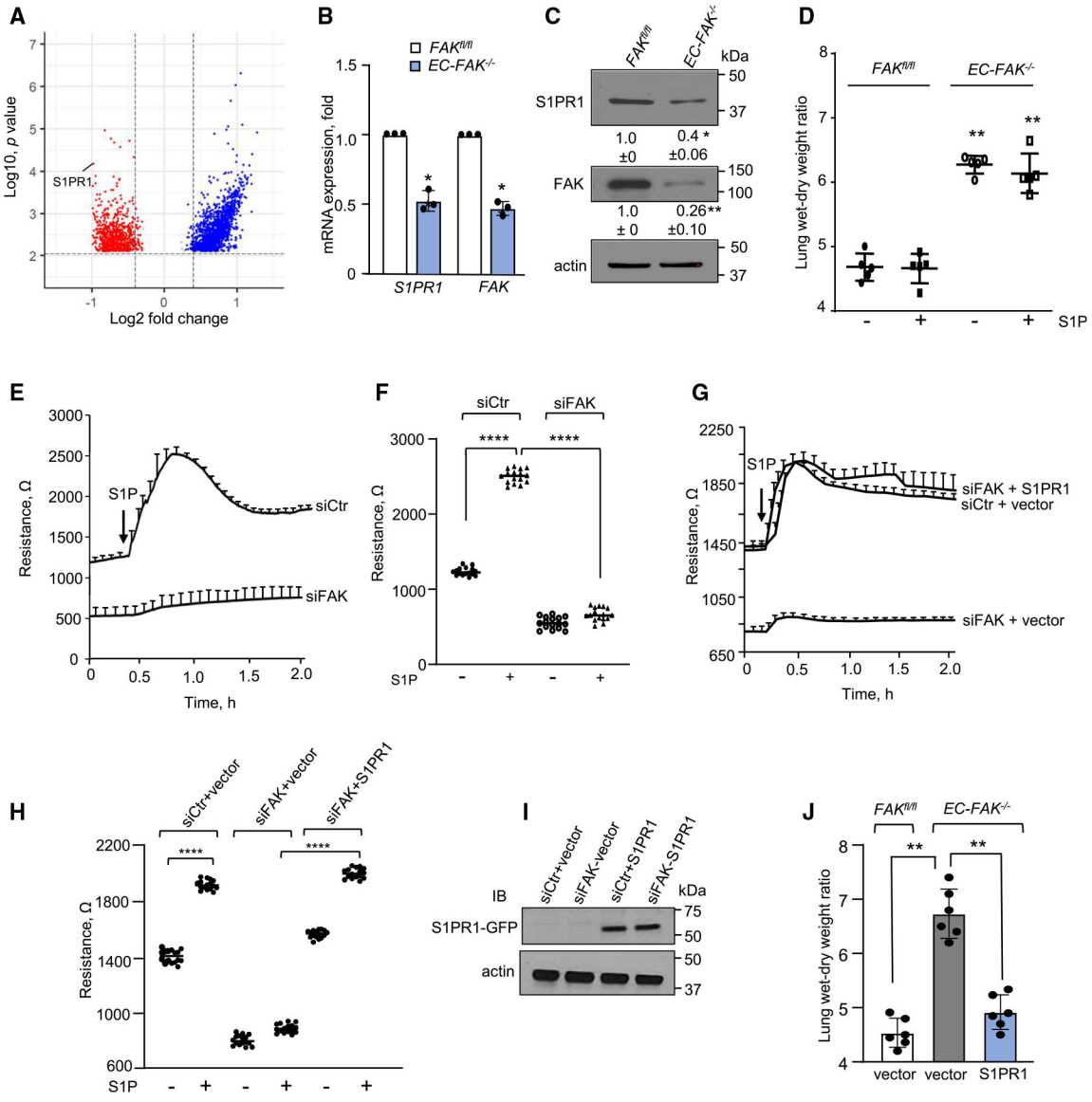

Figure 4. Transcriptome analysis identifies *S1PR1* as the gene of interest in maintaining vascular integrity downstream of FAK

(A–C) Volcano plot (A) of differential genes from bulk RNA-seq analysis of ECs sorted from *FAK*$^{fl/fl}$ and *EC-FAK*$^{-/-}$ mouse lungs. *S1PR1* mRNA (B) or protein (C) in FAK^{+} and FAK^{-} ECs using GAPDH as an internal mRNA control and actin as a loading control. Numbers indicate densitometric analysis (n = 3, unpaired t test).

(D) Lung edema 30 min after S1P (1 mg/kg, i.v.) administration in *FAK*$^{fl/fl}$ or *EC-FAK*$^{-/-}$ mice (n = 5 mice/group, one-way ANOVA with Tukey's *post hoc* test).

(E and F) TEER in control and FAK-depleted ECs at baseline and after adding 1 μM S1P. A representative trace from a single experiment with four wells/group is shown in (E), while (F) shows quantification pooled from four experiments (n = 4 wells/group) (one-way ANOVA with Tukey's *post hoc* test).

(G–I) Representative TEER trace in FAK-depleted ECs expressing vector or GFP-tagged WT-S1PR1 cDNA after addition of 1 μM S1P (n = 4 wells/group) is shown in (G), while

(H) shows quantification pooled from four sets of experiments ($n = 4$ wells/group). (I) A representative immunoblot of S1PR1 expression ($n = 3$). Actin was used as a loading control. The densitometric analysis could not be done as the GFP vector was undetected. (J) Lung edema in $FAK^{fl/fl}$ and $EC\text{-}FAK^{-/-}$ mice receiving vector or GFP-tagged WT-S1PR1 cDNA as in Figure 1F ($n = 6$ mice/group, one-way ANOVA with Tukey's *post hoc* test). Data are shown as individual values along with mean ± SEM. Statistical significance: *$p < 0.05$, **$p < 0.01$, ****$p < 0.0001$.

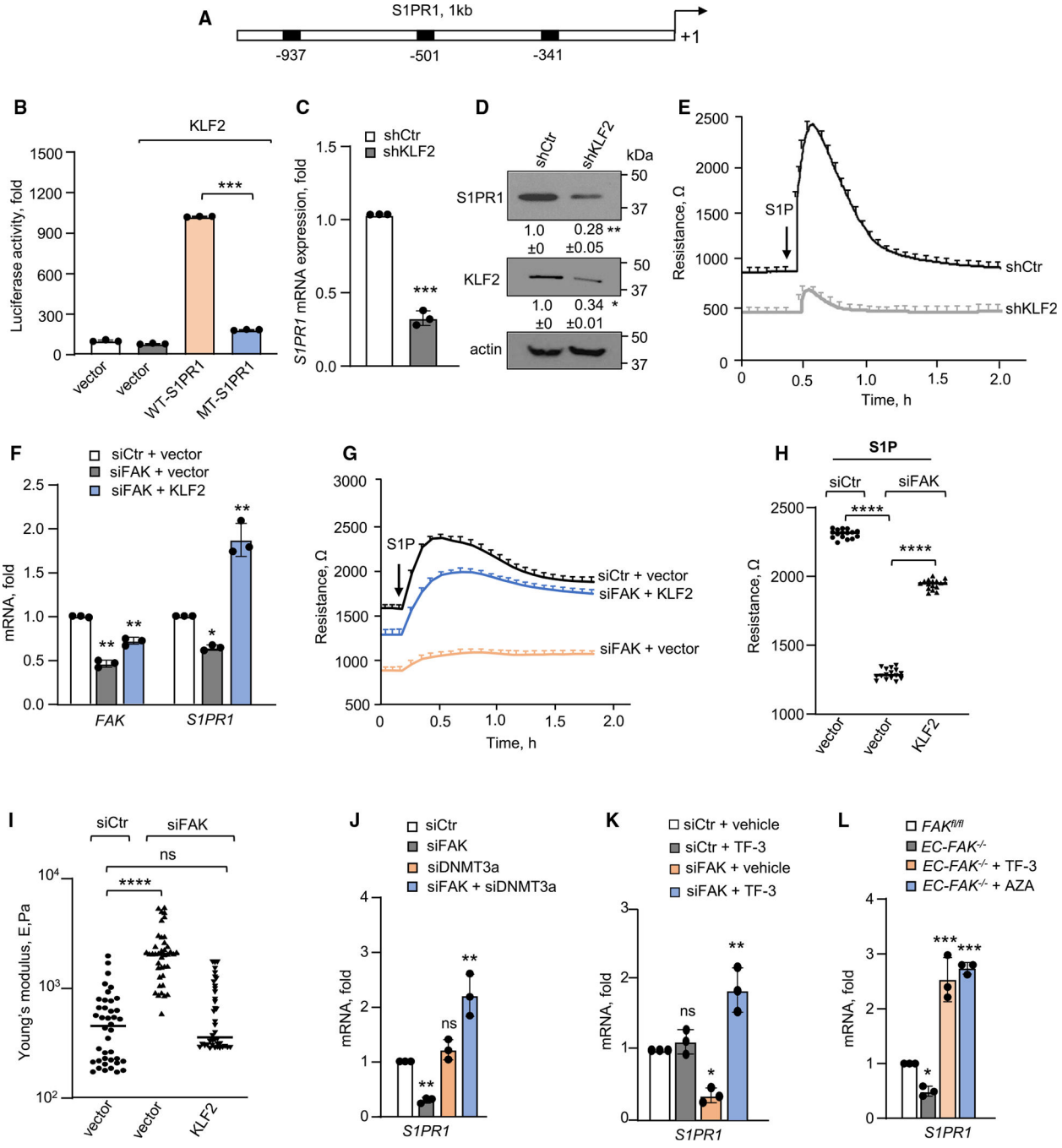

Figure 5. KLF2 regulates S1PR1 expression downstream of FAK

(A and B) Schematic representation of S1PR1 promoter with three KLF2 binding sites (−341, −501, and −937 from TSS) (A) and luciferase activity (B) in ECs co-transfecting KLF2 cDNA with WT- or mutated-S1PR1 luciferase promoter (which lacks three KLF2 binding sites) ($n = 3$; one-way ANOVA with Tukey's *post hoc* test).

(C and D) *S1PR1* mRNA (C) or protein expression (D) in control (shCtr) or KLF2-depleted ECs (shKLF2) using GAPDH as an internal control for mRNA and actin as a loading control. Numbers indicate densitometric analysis ($n = 3$, unpaired t test).

(E) A representative TEER trace in control or KLF2-depleted ECs after S1P (1 μM) addition. The experiments were repeated four times.
(F) *FAK* and *S1PR1* mRNA expression in FAK-depleted ECs, transducing KLF2 cDNA using GAPDH as an internal control ($n = 3$, one-way ANOVA with Tukey's *post hoc*).
(G and H) A representative TEER in control or FAK-depleted EC transducing vector or KLF2 cDNA (G). (H) Quantification of TEER pooled from four sets of experiments ($n = 4$ wells/group) (one-way ANOVA with Tukey's *post hoc* test).
(I) Young's modulus measurement in control or FAK-depleted ECs transducing vector or KLF2 cDNA using AFM by nanoscale indentation at 1 m/s. $N = 40$ cells/group, pooled from three independent experiments ($n = 3$, one-way ANOVA with Tukey's *post hoc* test).
(J and K) *S1PR1* mRNA in control, FAK-depleted, DNMT3a-depleted, and FAK+DNMT3a-depleted ECs (J) or following DNMT3a inhibition with 1 μM TF-3 for 4 h
(K). GAPDH was used as an internal control ($n = 3$, one-way ANOVA with Tukey's *post hoc* test).
(L) S1PR1 mRNA in $FAK^{fl/fl}$ and $EC\text{-}FAK^{-/-}$ mice 24 h after receiving 5-aza-2′-deoxycytidine (AZA) (0.5 mg/kg, i.v.) or TF-3 (1 mg/kg, i.v.). GAPDH was used as an internal control ($n = 3$, one-way ANOVA with Tukey's *post hoc* test).
Data scatter along with mean ± SEM. Statistical significance: $*p < 0.05$, $**p < 0.01$, $***p < 0.001$, $****p < 0.0001$; ns, not significant. Please see Figure S7.

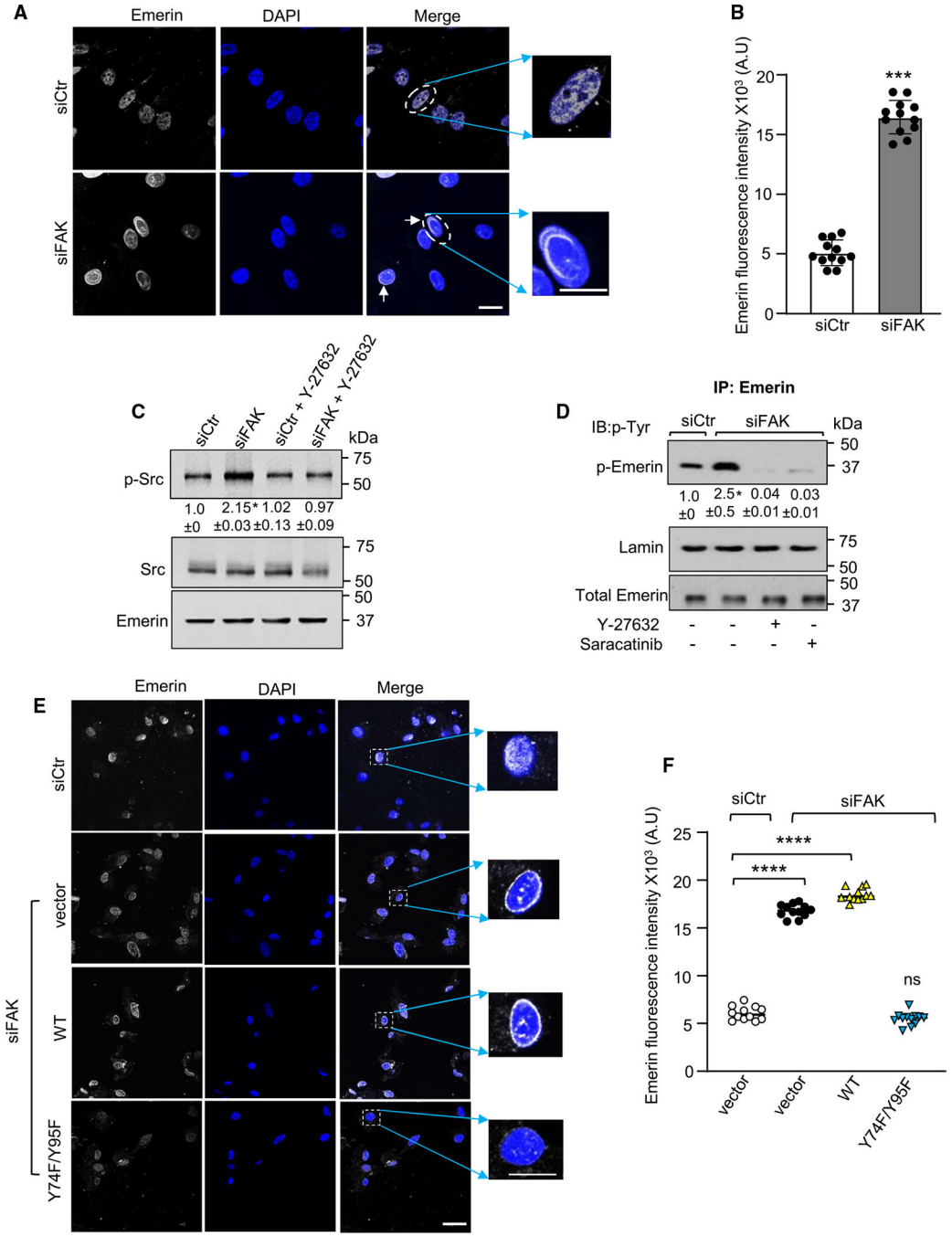

Figure 6. FAK regulates nuclear mechanotransduction by suppressing emerin activity

(A and B) A representative micrograph showing emerin localization in the nuclei of control or FAK-depleted ECs (A). Insets in (A) are magnified ×3. Scale bar: 20 μm for unmagnified images and 60 μm for magnified images. (B) A uniform area was drawn around the nuclear periphery in control or FAK-depleted ECs, and fluorescence intensity was quantified. Data are representative of at least $n = 12$ from experiments independently repeated three times (unpaired t test).

(C) cSrc-induced tyrosine phosphorylation in control or FAK-depleted ECs treated with Y-27632 (10 μM) as in Figure 1D or cSrc inhibitor (saracatinib, 100 nM, 2 h). An immunoblot with cSrc pan antibody was used to control protein loading. A representative blot is shown from experiments that were independently repeated three times. Numbers indicate densitometric analysis ($n = 3$, one-way ANOVA with Tukey's *post hoc* test).
(D) Emerin tyrosine phosphorylation in the nuclear fraction from control or FAK-depleted ECs after treatment with indicated inhibitors. Immunocomplexes wereimmunoblotted with p-Tyr (PY99/PY29, 1:250 dilution) to assess emerin tyrosine phosphorylation over total emerin and lamin. A representative immunoblot is shown from experiments that were repeated three times. Numbers indicate densitometric analysis ($n = 3$, one-way ANOVA with Tukey's *post hoc* test).
(E and F) Emerin reorganization in FAK-depleted ECs transducing WT or phospho-deficient emerin mutant (Y74F/Y95F) was determined as in (A). Scale bar: 20 μm for unmagnified images and 60 μm for magnified images. The fluorescence intensity of emerin was assessed as in (B) (data pooled from three individual experiments, one-way ANOVA with Tukey's *post hoc* test).
Data points show individual values along with mean ± SEM. Statistical significance: $*p < 0.05$, $***p < 0.001$, $****p < 0.0001$; ns, not significant.

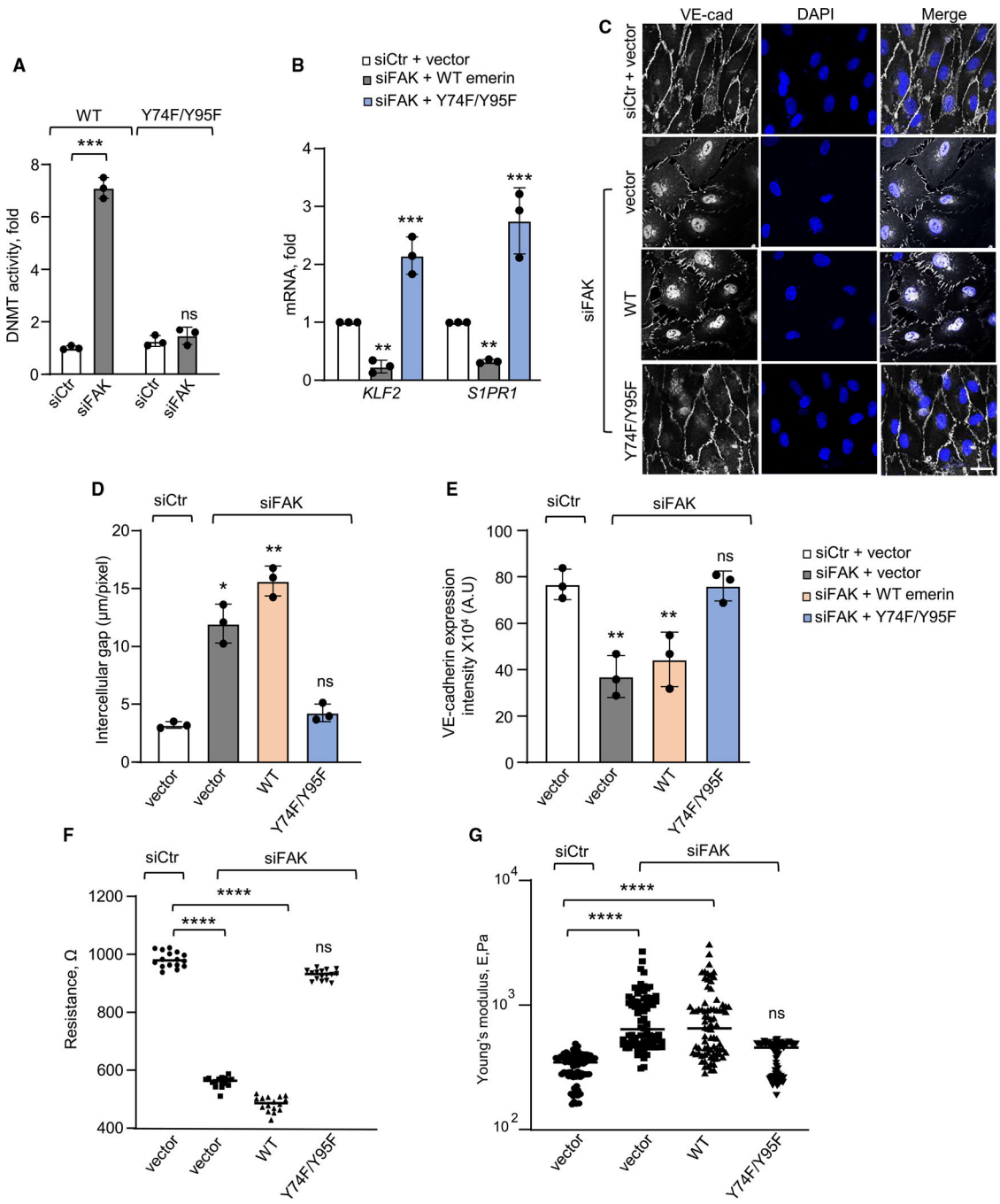

Figure 7. Suppression of emerin activity subverts restrictive EC fate

(A–E) DNMT activity (A), *KLF2* and *S1PR1* mRNA (B), and intercellular gaps measured by immunostaining with anti-VE-Cadherin antibody (C–E) in FAK-depleted ECs transducing WT or phosphor-defective emerin. GAPDH was used as an internal control for RNA in (B). Intercellular gap ($n = 3$) (D) and VE-cadherin fluorescence intensity (E) ($n = 3$, one-way ANOVA with Tukey's *post hoc* test for A, B, D, and E). Scale bar: 20 μm. (F and G) TEER (F) and Young's modulus (G) are in control or FAK-depleted ECs, transducing WT or phospho-deficient emerin mutants. (G) Quantification of TEER pooled

from four sets of experiments ($n = 4$ wells/group). $N = 40$ cells/group in (G) pooled from three independent experiments (one-way ANOVA with Tukey's *post hoc* test for F and G). Data expressed as mean ± SEM. Statistical significance: *$p < 0.05$, **$p < 0.01$, ***$p < 0.001$, ****$p < 0.0001$; ns, not significant.

Table 1.

Methylation-specific primers

Human *KLF2*	
Methylated	forward: 5’-AGAGTTTTTGAGAGGTTTCGATATC-3’ reverse: 5’-ACTACGACGACCTAAACCTTACG-3’
Unmethylated	forward: 5’-GAGAGTTTTTGAGAGGTTTTGATATT-3’ reverse: 5’-ACTACAACAACCTAAACCTTACACT-3’

Table 2.

Primers list

Genes	Human
FAK	forward: 5'-TGGGCGGAAAGAAATCCTGC-3' reverse: 5'-GGCTTGACACCCTCGTTGTA-3'
SOX17	forward: 5'-TTCGTGTGCAAGCCTGAGAT-3' reverse: 5'-TAATATACCGCGGAGCTGGC-3'
KLF2	forward: 5'-ACTCACACCTGCAGCTACGC-3' reverse: 5'-AGTGGTAGGGCTTCTCACCTGT-3'
FOXP1	forward: 5'-GCGGCAGCAACCACTTACTA-3' reverse: 5'-GTTTATGAGATGCCACTGTTGCT-3'
S1PR1	forward: 5'-AGCTCAGGGAACTTTGCGAG-3' reverse: 5'-GAGAAACAGCAGCCTCGCTC-3'
S1PR2	forward: 5'-CAACTCCGGGACATAGACCG-3' reverse: 5'-CATGGGGCTGAGCACTGG-3'
S1PR3	forward: 5'-CCTTGCAGAACGAGAGCCTAT-3' reverse: 5'-CCCGGAGAGTGTCATTTCCC-3'
DNMT3A	forward: 5'-GGCCATACGGTGGAGCC-3' reverse: 5'-TATCGTGGTCTTTGGAGGCG-3'
KLF4	forward: 5'-GGTCAGTCCCGGGGATTTGT-3' reverse: 5'-CAGTGGTAAGGTTTCTCACCTGTGT-3'
SPHK1	forward: 5'-GGCAGTCATGTCCGGTGATG-3' reverse: 5'-ACAGCAGTGTGCAGTTGATGA-3'
SPHK2	forward: 5'-CCCAGTGTTGGAGAGCTGAA 3' reverse: 5'-TGCTCCTCTGCTTCAAGGTG-3'
GAPDH	forward: 5'-AAGGTCATCCCAGAGCTGAA-3' reverse: 5'-CTGCTTCACCACCTTCTTGA-3'
Mouse	
FAK	forward: 5'-AATGAGGGTGTCAAGCCGTG-3' reverse: 5'-GGAGGAGCTGGCTGGATTTT-3'
SOX17	forward: 5'-CACCCCCACCCCAGTAAATC-3' reverse: 5'-GGAGGTGCTGCTCACTAGAT-3'
KLF2	forward: 5'-CTGCGTACACACACAGGTGAGAA-3' reverse: 5'-TCTGTTTGCAAGGGGACCG-3'
FOXP1	forward: 5'-CTCACTGCCTGTAGTGCCTC-3' reverse: 5'-GTCACGTCTCACCCCATTCA-3'
S1PR1	forward: 5'-ACTCTGACCAACAAGGAGATGCGTAC-3' reverse: 5'-GGCGATGATGGGTCGCTTGAATTT-3'
DNMT3A	forward: 5'-GGCCGAGGGCAGAGC-3' reverse: 5'-TCTTCCTTGCCACGGTTCTC-3'
GAPDH	forward: 5'-AATGGGCAGCCGTTAGGAAA-3' reverse: 5'-GCCCAATACGACCAAATCAGAG-3'

KEY RESOURCES TABLE

REAGENT or RESOURCE	SOURCE	IDENTIFIER
Antibodies		
CD31	BioLegend	Cat# 102409; RRID: AB_312904
CD45	BioLegend	Cat# 103114; RRID: AB_312979
S1PR1	Alomone labs	Cat# ASR-011; RRID: AB_2039836
Emerin	Cell Signaling Technology	Cat# 30853; RRID: AB_2798996
Src	Cell Signaling Technology	Cat# 2109; RRID: AB_2106059
p-Src	Cell Signaling Technology	Cat# 12432; RRID: AB_2797910
p-MLC	Cell Signaling Technology	Cat# 3671; RRID: AB_330248
FAK	Cell Signaling Technology	Cat# 3285; RRID: AB_2269034
p-FAK (Tyr397)	Cell Signaling Technology	Cat# 8556; RRID: AB_10891442
p-VE-Cadherin (Tyr731)	Thermo Fisher Scientific	Cat# 44-1145G; RRID: AB_2533584
GFP	Cell Signaling Technology	Cat# 2956; RRID: AB_1196615
Lamin A/C	Cell Signaling Technology	Cat# 2032; RRID: N/A
DNMT3a	Cell Signaling Technology	Cat# 3598; RRID: AB_2277449
DNMT3b	Santa Cruz Biotechnology	Cat# sc-7020; RRID: AB_2094125
DNMT1	Active Motif	Cat# 39204; RRID: AB_2614950
Phosphotyrosine (PY99)	Santa Cruz Biotechnology	Cat# 28692; RRID: AB_2798962
5-mC	Cell Signaling Technology	Cat# 28692; RRID: AB_2798962
ACTIN	Abclonal	Cat# AC026; RRID: AC026
CD31	Cell Signaling Technology	Cat# 3528; RRID: AB_2160882
KLF2	Abcam	Cat# Ab17008; RRID: AB_2890096
vWF	Abcam	Cat# ab11713; RRID:AB_298501
VE-Cadherin	Santa Cruz Biotechnology	Cat# sc-9989; RRID: AB_2077957
MEF-2	Santa Cruz Biotechnology	Cat# sc-17785; RRID: AB_627921
FC block CD16/32)	BioLegend	Cat# 101320; RRID: AB_1574975
Alexa Fluor 633 Phalloidin	Thermo Fisher Scientific	Cat# A22284; RRID: N/A
Alexa Fluor 647	Thermo Fisher Scientific	Cat# A-21245; RRID: AB_141775
Alexa Fluor 633	Thermo Fisher Scientific	Cat# A-21070; RRID: AB_2535731
Alexa Fluor 488	Thermo Fisher Scientific	Cat# A-11001; RRID: AB_2534069
Alexa Fluor 488	Thermo Fisher Scientific	Cat# A-11008; RRID: AB_143165
Alexa Fluor 594	Thermo Fisher Scientific	Cat# A-11016; RRID: AB_2534083
Anti-rabbit IgG, HRP-linked Antibody	Cell Signaling Technology	Cat# 7074; RRID: AB_2099233
Anti-mouse IgG, HRP-linked Antibody	Cell Signaling Technology	Cat# 7076; RRID: AB_330924
Rabbit IgG Isotype Control	Thermo Fisher Scientific	Cat# 02-6102; RRID: AB_2532938
Sheep IgG Isotype Control	Thermo Fisher Scientific	Cat# 31243; RRID: AB_243595
Chemicals, peptides, and recombinant proteins		
Sphingosine-1-phosphate	Enzo life Inc	BML-SL140-001
DAPI	Thermo Fisher Scientific	Cat# D-1306

REAGENT or RESOURCE	SOURCE	IDENTIFIER
RhoA activation assay	Cytoskeleton Inc	Cat# BK036-S
Fast SYBR green mastermix	Applied Biosystems	Cat# 4385612
High-capacity cDNA reverse transcription kit	Applied Biosystems	Cat# 4368814
PF-562271	Selleckchem	Cat# S2013
Blebbistatin	Cayman Chemical	Cat# 13013
Y-27632	Cayman Chemical	Cat# 0005583
Theaflavin 3,3′-digallate	Cayman Chemical	Cat# 25215
5-Aza-2′-deoxycytidine	MilliporSigma	Cat# A3565
Saracatinib	Santa Cruz Biotechnology	Cat# 379231-04-6
Tamoxifen	MilliporSigma	Cat# T5648
Corn oil	MilliporeSigma	Cat# C8267
Citrate-based antigen unmasking solution	Vector laboratories	Cat# H-3300
EGM-2	Lonza Bioscience	Cat# CC-3162
Lipopolysaccharide	Millipore Sigma	Cat# L2880
siRNA Transfection Reagent	Santa Cruz Biotechnology	Cat# sc-29528
Plasmid transfection medium	Santa Cruz Biotechnology	Cat# sc-108062
AMAXA nucleofection	Lonza Bioscience	Cat# VPI-1001
FuGENE HD transfection reagent	Promega	Cat# E2311
Cell contraction assay	Cell Biolabs, Inc	Cat# CBA-201
DNA clean & concentrator 5	Zymo Research	Cat# D4013
Genomic DNA kit	Qiagen	Cat# 59124
pGEM-T Easy Vector System	Promega	Cat# A1360
NE-PER™ Nuclear and Cytoplasmic Extraction Reagents	Thermo Fisher Scientific	Cat# 78833
DNA methyltransferase activity assay	EpiGenTek	Cat# P-3001-1
TEER electrodes	Applied Biophysics, Inc.	Cat# 8W10E+
Collagenase	Roche	Cat# 10103578001
Collagenase	Roche	Cat# 10103578001
Catalse	MilliporeSigma	Cat# C-40
Glucose oxidase	MilliporeSigma	Cat# G2133
Trizol	Thermo Fisher Scientific	Cat# 15596026
Prolong Gold antifade	Invitrogen	Cat# P36934
Cys-RGD peptide	Peptide 2.0	https://pubmed.ncbi.nlm.nih.gov/34677951/
Deposited data		
RNA-seq	GEO	GSE212037
ATAC-seq	GEO	GSE207789
Experimental models: Cell lines		
Primary Human Pulmonary Artery Endothelial Cells (HPAE)	Lonza Bioscience	Cat# CC-2530
Experimental models: Organisms/strains		

REAGENT or RESOURCE	SOURCE	IDENTIFIER
FAK$^{fl/fl}$	Dr. Jun-Lin Guan Lab	https://pubmed.ncbi.nlm.nih.gov/15967814/
EC-FAK$^{-/-}$	This paper	N/A
tdTom-EC	This paper	N/A
tdTom-EC-FAK$^{-/-}$	This paper	N/A
Wild type	This paper	N/A
Oligonucleotides		
Human KLF2 Methylated:Forward - 5'-AGAGTTTTTGAGAGGTTTCGATATC-3' Reverse - 5'-ACTACGACGACCTAAACCTTACG-3'	This paper	N/A
Human KLF2 Unmethylated: Forward - 5'-GAGAGTTTTTGAGAGGTTTTGATATT-3' Reverse - 5'-ACTACAACAACCTAAACCTTACACT-3'	This paper	N/A
qRT-PCR primers used in this study	This paper	See Table S1
Recombinant DNA		
WT-FAK	Dr. Mehta lab, UIC	https://pubmed.ncbi.nlm.nih.gov/23771883/
KD-FAK	Dr. Karginov lab, UIC	N/A
WT-RhoA	This paper	N/A
Q63L-RhoA	This paper	N/A
DN-RhoA	Dr. Mehta lab, UIC	N/A
SOX17	Dr. Rehman lab, UIC	https://pubmed.ncbi.nlm.nih.gov/31073164/
WT-emerin	Dr. Guilluy lab	https://pubmed.ncbi.nlm.nih.gov/24609268/
Emerin Y74F/Y95F	Dr. Guilluy lab	https://pubmed.ncbi.nlm.nih.gov/24609268/
Software and algorithms		
OMX-SoftWoRx	DeltaVision OMX SR	N/A
QUMA	Dr. Okano lab	https://pubmed.ncbi.nlm.nih.gov/18487274/
Integrative Genomics Viewer	Broad Institute	N/A
Fiji (ImageJ)	NIH	https://imagej.net/Fiji
GraphPad Prism Version 8	Dotmatics	https://www.graphpad.com/scientific-software/prism/
FlowJo	BD Biosciences	N/A
Imaris image analysis	Oxford Instruments	N/A
Biorender	Biorender	N/A